Ukrainian Journal of Physical Optics
ISSUE 3
2026

Highly Dispersive Optical Solitons with Differential Group Delay and Multiplicative White Noise Having Kerr Law of Self-Phase Modulation

Ahmed S. M. Metwally [1], Mohamed E. M. Alngar [2], Reham M. A. Shohib [3], Syed A. A. Shah [4], Anjan Biswas [5,6,7,8,9] *

[1] Center of Excellence for Research in Science and Mathematics Education Development, DSR, King Saud University, P.O. Box 11451, Riyadh, Saudi Arabia
[2] Mathematics Education Program, Faculty of Education and Arts, Sohar University, Sohar 311, Oman
[3] Basic Science Department, Faculty of Economics and Business Administration, Innovation University, Sharqia, Egypt
[4] Department of Modern Mechanics, School of Engineering Science, University of Science and Technology of China, Hefei, 230026, China
[5] Department of Mathematics & Physics, Grambling State University, Grambling, LA 71245–2715, USA
[6] Department of Mathematics, Faculty of Science, Karadeniz Technical University, Trabzon–61080, Turkiye
[7] Department of Physics and Electronics, Khazar University, Baku, AZ–1096, Azerbaijan
[8] Applied Science Research Center, Applied Science Private University, Amman–11937, Jordan
[9] Department of Mathematics and Applied Mathematics, Sefako Makgatho Health Sciences University, Medunsa–0204, Pretoria, South Africa
* Corresponding author: biswas.anjan@gmail.com

Received: 17.07.2026

Abstract. This work presents a comprehensive analytical investigation of stochastic optical solitons propagating in highly dispersive birefringent fibers governed by Kerr-law refractive-index nonlinearity in the Itô sense. Starting from a coupled stochastic nonlinear Schrödinger system including high-order dispersion, cross-phase modulation, and Wiener-induced phase fluctuations, a traveling-wave reduction is employed to obtain a deterministic ordinary differential equation for the soliton envelopes after imposing appropriate constraint conditions. Using the modified subsidiary ordinary differential equation sub-ODE method, we derive several families of exact closed-form solutions, including bright, dark, singular, and Weierstrass elliptic structures, together with their corresponding existence conditions. The bright and dark soliton solutions are subsequently analyzed to illustrate the effects of stochastic perturbation. The analytical results reveal how the hierarchy of higher-order dispersion interacts with Kerr nonlinearity to stabilize localized waveforms, while the Itô stochastic term modifies only the internal phase without affecting the soliton modulus. Furthermore, the obtained soliton families satisfy the derived stability conditions, demonstrating that the envelope profiles remain robust despite the presence of multiplicative white noise. These findings provide new insight into noise-driven nonlinear wave propagation in birefringent optical fibers and offer exact analytical benchmarks for ultrafast photonics, nonlinear pulse management, and stochastic optical systems.

Keywords: optical solitons, high-order dispersion, birefringent fibers, Kerr nonlinearity, Itô calculus, stochastic nonlinear Schrödinger equation, modified method of subsidiary ordinary differential equation
UDC: 535.3
DOI: 10.3116/16091833/Ukr.J.Phys.Opt.2026.03196

1. Introduction

Optical solitons are self-sustaining nonlinear wave packets that preserve their shape during propagation because of a precise balance between dispersion and nonlinear self-phase modulation [1,2]. Since their discovery, solitons have played a fundamental role in nonlinear optics and have become essential in modern photonic applications such as high-speed communication, ultrafast optical processing, and nonlinear waveguiding technologies [3-5].

In birefringent optical fibers, the propagation dynamics become considerably richer, as two orthogonal polarization components interact through cross-phase modulation and higher-order dispersion, giving rise to vector solitons, polarization rotation, and complex multi-component nonlinear structures [6-8]. For ultrashort optical pulses, the standard NLSE fails to capture the underlying dynamics because higher-order dispersion, self-steepening, and material-induced corrections become significant [9-11]. Extended nonlinear Schrödinger equation NLSE models that include these higher-order effects have been widely analyzed, particularly in studies that systematically explored Kerr-type nonlinear systems with dispersive hierarchies [12-14]. Kerr-law nonlinearity remains a primary mechanism in such media, and its role in soliton formation has been extensively documented in various nonlinear contexts [15,16].

Real fiber systems, however, are never perfectly deterministic. Noise arising from thermal fluctuations, manufacturing imperfections, fiber birefringence randomness, and amplifier-induced perturbations introduces stochastic variations into the propagating optical fields [17,18]. Stochastic NLSE models formulated in the Itô sense have therefore become vital for describing noise-driven phase diffusion, coherence degradation, and soliton stability under random perturbations [19,20]. Recent studies have shown that stochastic perturbations can strongly affect the soliton phase while leaving the amplitude profile essentially intact [21,22]. However, these investigations were primarily restricted to simpler stochastic nonlinear Schrödinger models and did not address coupled birefringent systems incorporating the complete hierarchy of higher-order dispersion together with Kerr-law nonlinear interactions. Motivated by this gap, the present work develops a coupled stochastic high-order NLSE model for birefringent optical fibers and derives exact analytical families of bright, dark, singular, and Weierstrass elliptic vector soliton solutions using the modified sub-ODE method. In addition to establishing the corresponding compatibility and existence conditions, the analysis demonstrates that the phase-preserving effect of Itô stochastic perturbations remains valid even in this significantly more general high-order framework.

The present article investigates a coupled stochastic NLSE system that incorporates the full hierarchy of high-order dispersion and Kerr-type nonlinear interactions in birefringent fibers. This framework extends several analytical models that have contributed significantly to high-order NLSE soliton theory and exact analytical methodologies [23,24].

To derive explicit analytical solutions, we employ the modified sub-ODE method [24,25], a powerful technique that has been refined and applied to a wide class of nonlinear evolution equations. Using this framework, we obtain families of bright, dark, singular, periodic, and Weierstrass elliptic solutions, representing a broad spectrum of nonlinear behaviors arising from the interplay between dispersion hierarchy, Kerr nonlinearity, and stochastic phase modulation.

Beyond their mathematical significance, these solutions provide physical insight into noise-modulated soliton dynamics in birefringent Kerr media. The analytical results demonstrate that, for the coupled stochastic high-order birefringent Kerr-law model considered in this work, the Itô stochastic perturbation modifies only the soliton phase while leaving the envelope modulus unchanged. This extends the phase-preserving property previously reported for simpler stochastic nonlinear optical models to a more general birefringent system incorporating the full hierarchy of higher-order dispersion. This indicates a notable degree of robustness that is highly relevant for practical fiber-optic communication and ultrafast photonic applications.

This paper is organized as follows. Section 2 presents the mathematical formulation of the coupled stochastic nonlinear Schrödinger model describing highly dispersive optical solitons in birefringent fibers under Kerr-law nonlinearity in the Itô sense. Section 3 develops the analytical framework by employing a traveling-wave reduction and deriving the associated compatibility conditions. Section 4 outlines the modified Sub-ODE method and constructs several families of exact analytical solutions, including bright, dark, singular, and Weierstrass elliptic solitons, together with the corresponding existence constraints. Section 5 discusses the physical interpretation and stability characteristics of the obtained soliton solutions. Finally, Section 6 summarizes the main findings and highlights their significance for stochastic nonlinear optical systems.

2. Mathematical model

The dimensionless coupled stochastic NLSE considered in this work is formulated by extending the deterministic high-order birefringent Kerr-law model to include multiplicative Itô white-noise perturbations. The deterministic terms follow the standard high-order dispersion hierarchy and Kerr nonlinear interactions reported in the literature [26–28], while the stochastic contribution is introduced here to account for random phase fluctuations. The resulting governing equations are given by

$$\begin{aligned}&iQ_t + ia_{11}Q_x + a_{12}Q_{xx} + ia_{13}Q_{xxx} + a_{14}Q_{xxxx}\\&+ia_{15}Q_{xxxxx} + a_{16}Q_{xxxxxx} + \left(b_{14}|Q|^2 + b_{15}|R|^2\right)Q + \sigma Q\frac{dW}{dt} = 0,\end{aligned}\tag{1}$$

$$\begin{aligned}&iR_t + ia_{21}R_x + a_{22}R_{xx} + ia_{23}R_{xxx} + a_{24}R_{xxxx}\\&+ia_{25}R_{xxxxx} + a_{26}R_{xxxxxx} + \left(b_{24}|R|^2 + b_{25}|Q|^2\right)R + \sigma R\frac{dW}{dt} = 0.\end{aligned}\tag{2}$$

The dimensionless NLSE system describes the evolution of the two polarization components $Q(x,t)$ and $R(x,t)$ in a birefringent fiber with high dispersion and Kerr-law refractive-index nonlinearity. The coefficients a_{1j} and a_{2j} ($j = 1,\ldots,6$) represent the dispersion hierarchy: the terms with odd-order spatial derivatives correspond to dispersive effects, while the even-order derivatives account for higher-order corrections associated with material and waveguide dispersion in each polarization mode. The nonlinear coefficients b_{14}, b_{15}, b_{24} and b_{25} describe self-phase modulation and cross-phase modulation between the two polarization components, reflecting the Kerr response of the medium. The parameter σ denotes the strength of the stochastic perturbation, and the term (dW/dt) represents white noise obtained as the formal time derivative of a Wiener process $W(t)$, modeling random fluctuations in birefringence or refractive index. This stochastic contribution is included in the Itô sense and affects only the phase of the complex fields.

We use the Itô interpretation because the stochastic perturbation is intended to represent rapid, memoryless (white) fluctuations with independent increments, for which Itô calculus provides the natural framework for analysis and Monte-Carlo simulation. A direct consequence is the Itô drift correction in the phase, giving the term $\sigma W(t) - \sigma^2 t$ in the exact solution ansatz; physically, this corresponds to phase diffusion (coherence loss) while the modulus remains controlled by the deterministic dispersion-nonlinearity balance.

3. Preliminary analysis

In this section, we will suppose that Eqs. (1) and (2) possess the following solutions:

$$\begin{aligned} Q(x,t) &= \phi_1(z)\ \exp\left[i\left(-\kappa x + \omega t + \sigma W - \sigma^2 t\right)\right] \\ R(x,t) &= \phi_2(z)\ \exp\left[i\left(-\kappa x + \omega t + \sigma W - \sigma^2 t\right)\right], \end{aligned} \tag{3}$$

and

$$z = x - vt. \tag{4}$$

Here, $\phi_1(z)$ and $\phi_2(z)$ denote the soliton envelopes of the two polarization components, expressed in the retarded coordinate $z = x - vt$ that moves with the pulse at the group velocity v. The parameters κ and ω represent the wave number and the carrier frequency, respectively. The additional term $\left(-\sigma^2 t\right)$ in the phase is the Itô correction associated with the multiplicative Wiener process, and it ensures that the stochastic perturbation produces phase-only modulation without changing the mean optical power. The ansatz in Eq. (3) is therefore adopted to construct soliton-type (shape-preserving) traveling-wave solutions: by enforcing dependence on z only, the coupled stochastic evolution equations reduce to a set of ordinary differential equations for $\phi_{1,2}(z)$. This reduction is valid provided the real/imaginary-part decomposition is consistent, which yields the required parameter relations and constraint conditions derived later in the manuscript.

Substituting (3) and (4) into Eqs. (1) and (2) and isolating their real and imaginary parts, one gets:

$$\begin{aligned} \Re_1:\ & a_{16}\phi_1^{(6)}(z) + \left(a_{14} + 5a_{15}\kappa - 15a_{16}\kappa^2\right)\phi_1^{(4)}(z) \\ & + \left(a_{12} + 3a_{13}\kappa - 6a_{14}\kappa^2 - 10a_{15}\kappa^3 + 15a_{16}\kappa^4\right)\phi_1''(z) \\ & + \left(\sigma^2 - \omega + a_{11}\kappa - a_{12}\kappa^2 - a_{13}\kappa^3 + a_{14}\kappa^4 + a_{15}\kappa^5 - a_{16}\kappa^6\right)\phi_1(z) \\ & + b_{14}\phi_1^3(z) + b_{15}\phi_1(z)\phi_2^2(z) = 0, \end{aligned} \tag{5}$$

$$\begin{aligned} \Re_2:\ & a_{26}\phi_2^{(6)}(z) + \left(a_{24} + 5a_{25}\kappa - 15a_{26}\kappa^2\right)\phi_2^{(4)}(z) \\ & + \left(a_{22} + 3a_{23}\kappa - 6a_{24}\kappa^2 - 10a_{25}\kappa^3 + 15a_{26}\kappa^4\right)\phi_2''(z) \\ & + \left(\sigma^2 - \omega + a_{21}\kappa - a_{22}\kappa^2 - a_{23}\kappa^3 + a_{24}\kappa^4 + a_{25}\kappa^5 - a_{26}\kappa^6\right)\phi_2(z) \\ & + b_{24}\phi_2^3(z) + b_{25}\phi_1^2(z)\phi_2(z) = 0, \end{aligned} \tag{6}$$

and

$$\begin{aligned} \Im_1:& \left(a_{15} - 6a_{16}\kappa\right)\phi_1^{(5)}(z) + \left(a_{13} - 4a_{14}\kappa - 10a_{15}\kappa^2 + 20a_{16}\kappa^3\right)\phi_1'''(z) \\ & -(v - a_1 1 + 2a_{12}\kappa + 3a_{13}\kappa^2 - 4a_1 4\kappa^3 - 5a_{15}\kappa^4 + 6a_{16}\kappa^5)\phi_1'(z) = 0, \end{aligned} \tag{7}$$

$$\begin{aligned} \Im_2:& \left(a_{25} - 6a_{26}\kappa\right)\phi_2^{(5)}(z) + \left(a_{23} - 4a_{24}\kappa - 10a_{25}\kappa^2 + 20a_{26}\kappa^3\right)\phi_2'''(z) \\ & -\left(v - a_{21} + 2a_{22}\kappa + 3a_{23}\kappa^2 - 4a_{24}\kappa^3 - 5a_{25}\kappa^4 + 6a_{26}\kappa^5\right)\phi_2'(z) = 0. \end{aligned} \tag{8}$$

Set

$$\phi_2(z) = C\phi_1(z), \tag{9}$$

where C is a nonzero real constant representing the amplitude ratio between the two polarization components. The restriction $C \neq 0$ ensures that both polarization components are present, whereas $C = 0$ reduces the system to a single-component model. The special case

C = 1, corresponding to equal-amplitude polarization components, is also admissible. Under this assumption, Eqs. (5)–(8) become

$$\begin{aligned}&\Re_1: a_{16}\phi_1^{(6)}(z)+\left(a_{14}+5a_{15}\kappa-15a_{16}\kappa^2\right)\phi_1^{(4)}(z)\\&+\left(a_{12}+3a_{13}\kappa-6a_{14}\kappa^2-10a_{15}\kappa^3+15a_{16}\kappa^4\right)\phi_1''(z)\\&+\left(\sigma^2-\omega+a_{11}\kappa-a_{12}\kappa^2-a_{13}\kappa^3+a_{14}\kappa^4+a_{15}\kappa^5-a_{16}\kappa^6\right)\phi_1(z)\\&+(b_{1}4+C^2b_{1}5)\phi_1^3(z)=0,\end{aligned} \tag{10}$$

$$\begin{aligned}&\Re_2: a_{26}\phi_1^{(6)}(z)+\left(a_{24}+5a_{25}\kappa-15a_{26}\kappa^2\right)\phi_1^{(4)}(z)\\&+\left(a_{22}+3a_{23}\kappa-6a_{24}\kappa^2-10a_{25}\kappa^3+15a_{26}\kappa^4\right)\phi_1''(z)\\&+\left(\sigma^2-\omega+a_{21}\kappa-a_{22}\kappa^2-a_{23}\kappa^3+a_{24}\kappa^4+a_{25}\kappa^5-a_{26}\kappa^6\right)\phi_1(z)\\&+\left(b_{24}C^2+b_{25}\right)\phi_1^3(z)=0,\end{aligned} \tag{11}$$

and

$$\begin{aligned}&\Im_1: \left(a_{15}-6a_{16}\kappa\right)\phi_1^{(5)}(z)+\left(a_{13}-4a_{14}\kappa-10a_{15}\kappa^2+20a_{16}\kappa^3\right)\phi_1'''(z)\\&-\left(v-a_{11}+2a_{12}\kappa+3a_{13}\kappa^2-4a_{14}\kappa^3-5a_{15}\kappa^4+6a_{16}\kappa^5\right)\phi_1'(z)=0,\end{aligned} \tag{12}$$

$$\begin{aligned}&\Im_2: \left(a_{25}-6a_{26}\kappa\right)\phi_1^{(5)}(z)+\left(a_{23}-4a_{24}\kappa-10a_{25}\kappa^2+20a_{26}\kappa^3\right)\phi_1'''(z)\\&-\left(v-a_{21}+2a_{22}\kappa+3a_{23}\kappa^2-4a_{24}\kappa^3-5a_{25}\kappa^4+6a_{26}\kappa^5\right)\phi_1'(z)=0.\end{aligned} \tag{13}$$

By equating the coefficients of the linearly independent functions in Eqs. (12) and (13) to zero, we obtain:

$$\kappa=\frac{a_{j5}}{6a_{j6}},\ j=1,2, \tag{14}$$

$$v=a_{j1}-2a_{j2}\kappa-3a_{j3}\kappa^2+4a_{j4}\kappa^3+5a_{j5}\kappa^4-6a_{j6}\kappa^5,\ j=1,2, \tag{15}$$

$$a_{j3}-4a_{j4}\kappa-10a_{j5}\kappa^2+20a_{j6}\kappa^3=0,\ j=1,2. \tag{16}$$

Eqs. (10) and (11) exhibit identical forms under the following constraint conditions:

$$\left.\begin{aligned}a_{16}-a_{26}&=0,\\a_{14}-a_{24}+5\left(a_{15}-a_{25}\right)\kappa-15\left(a_{16}-a_{26}\right)\kappa^2&=0,\\a_{12}-a_{22}+3\left(a_{13}-a_{23}\right)\kappa-6\left(a_{14}-a_{24}\right)\kappa^2&\\-10\left(a_{15}-a_{25}\right)\kappa^3+15\left(a_{16}-a_{26}\right)\kappa^4&=0,\\\left(a_{11}-a_{21}\right)\kappa-\left(a_{12}-a_{22}\right)\kappa^2-\left(a_{13}-a_{23}\right)\kappa^3&\\+\left(a_{14}-a_{24}\right)\kappa^4+\left(a_{15}-a_{25}\right)\kappa^5-\left(a_{16}-a_{26}\right)\kappa^6&=0,\\b_{14}-b_{25}+C^2\left(b_{15}-b_{24}\right)&=0.\end{aligned}\right\} \tag{17}$$

We can express Eq. (10) in an alternative form as follows:

$$\phi_1^{(6)}(z)+\Delta_1\phi_1^{(4)}(z)+\Delta_2\phi_1''(z)+\Delta_3\phi_1(z)+\Delta_4\phi_1^3(z)=0, \tag{18}$$

where

$$\left.\begin{aligned}&\Delta_1=\frac{a_{14}+5a_{15}\kappa-15a_{16}\kappa^2}{a_{16}},\quad \Delta_2=\frac{a_{12}+3a_{13}\kappa-6a_{14}\kappa^2-10a_{15}\kappa^3+15a_{16}\kappa^4}{a_{16}},\\&\Delta_3=\frac{\sigma^2-\omega+a_{11}\kappa-a_{12}\kappa^2-a_{13}\kappa^3+a_{14}\kappa^4+a_{15}\kappa^5-a_{16}\kappa^6}{a_{16}},\ \Delta_4=\frac{b_{14}+C^2b_{15}}{a_{16}}.\end{aligned}\right\} \tag{19}$$

The relations in Eqs. (14)-(17) arise as compatibility conditions when one seeks a class of shape-preserving traveling-wave solutions with a common carrier phase for the coupled polarization system. Eqs. (14)-(16) follow from the consistency of the imaginary-part equations, while Eq. (17) is required for the two real-part envelope equations to assume an identical form and hence reduce to the single scalar ODE (18).

4. Modified sub-ODE method

In this section, we briefly explain the modified Sub-ODE method that we employ to construct closed-form traveling-wave solutions of the reduced nonlinear ODE (18). The method is constructive: it converts the nonlinear ODE into an algebraic system by representing the unknown envelope as a finite expansion in terms of an auxiliary function satisfying a simpler first-order equation. Such auxiliary-equation approaches are widely used to generate analytic soliton, singular-soliton, and periodic/elliptic solutions for nonlinear wave equations. The modified Sub-ODE method proceeds through the following steps.

Step 1: We seek solutions of Eq. (18) in the form of a finite polynomial expansion

$$\phi_1(z)=\sum_{j=0}^{m}\alpha_j f^j(z), \tag{20}$$

where $\alpha_j\left(j=0,1,2,\ldots,m\right)$ are constants to be determined, with $\alpha_m\neq 0$ to ensure that the expansion is truly of order m. The integer m is not chosen arbitrarily; it is fixed by a dominant-balance (homogeneous balance) argument so that the ansatz contains enough terms to accommodate the highest derivative contribution and the strongest nonlinearity in Eq. (18).

Step 2: The auxiliary function $f(z)$ is assumed to satisfy the first-order Sub-ODE:

$$f'(z)=\sqrt{\rho_0 f^{2-2n}(z)+\rho_1 f^{2-n}(z)+\rho_2 f^{2}(z)+\rho_3 f^{2+n}(z)+\rho_4 f^{2+2n}(z)}, \tag{21}$$

where $\rho_l\left(l=0,1,2,3,4\right)$ are constants and $n>0$. This sub-ODE is sufficiently general to generate hyperbolic (soliton), trigonometric (periodic), and elliptic-function families, depending on the parameter selection. The presence of the exponent parameter n is a key feature of the modified approach: it allows the auxiliary equation to produce solution profiles with adjustable steepness and background behavior, which is useful when constructing bright, dark, and singular solutions from the same unified framework.

Step 3: To systematically determine m and organize the coefficient-matching process, we use the degree operator $D[\cdot]$ with the convention $D[f]=n$ and $D\left[\alpha_j\right]=0$ for constants. From Eq. (20), the dominant contribution is $\phi_1\sim\alpha_m f^m$, hence $D\left[\phi_1(z)\right]=m$. Using Eq. (21), one obtains that each differentiation increases the degree by n, leading to

$$D\left[\phi_1'(z)\right]=m+n,\ D\left[\phi_1''(z)\right]=m+2n, \tag{22}$$

and, more generally,

$$D\left[\phi_1^{(r)}(z)\right]=m+rn,\ D\left[\phi_1^{(r)}(z)\phi_1^{s}(z)\right]=(s+1)m+nr, \tag{23}$$

These relations are then used to select m by balancing the degree of the highest-order derivative term in Eq. (18) with the degree of the strongest nonlinear term. Once m is fixed, the ansatz (20) is fully specified.

Step 4: We substitute Eq. (20) into Eq. (18). Derivatives $\phi_1^{(r)}(z)$ generate terms involving $f^j(z)$ and derivatives of $f(z)$. The sub-ODE (21) is then used repeatedly to eliminate $f'(z)$ (and higher derivatives obtained by differentiating Eq. (21)) so that Eq. (18) becomes an algebraic identity in powers of $f(z)$, one gets algebraic system for the unknown constants α_j and the sub-ODE parameters ρ_l (and possibly n), together with relations among the physical coefficients appearing in Eq. (18). Solving this algebraic system yields explicit solution families.
Step 5: Once $\phi_1(z)$ is obtained, the corresponding fields are reconstructed using the traveling-wave representation introduced earlier. Different parameter choices yield bright solitons, dark solitons, singular solitons, and elliptic solutions.

It should be emphasized that the parameters ρ_l ($l=0,\ldots,4$) are auxiliary constants introduced by the modified sub-ODE method and do not represent independent physical quantities of the optical fiber model. Their values are determined by solving the algebraic system obtained after substituting the polynomial ansatz into the reduced governing equation. Therefore, they are implicitly related to the physical coefficients governing dispersion, Kerr nonlinearity, and the wave parameters through the compatibility conditions. Different admissible choices of the auxiliary parameters correspond to different mathematical solution branches, which, in turn, describe distinct physical wave structures such as bright, dark, singular, and elliptic solitons.

Family 1. If $\rho_0=\rho_1=\rho_3=0$, Eq. (21) reduces to $f'(z)=f(z)\sqrt{\rho_2+\rho_4 f^{2n}(z)}$, which admits the following hyperbolic solutions:

(I) Bright soliton:

$$f(z)=\left[\pm\sqrt{-\frac{\rho_2}{\rho_4}}\operatorname{sech}\left(n\sqrt{\rho_2}z\right)\right]^{\frac{1}{n}},\quad \rho_2>0,\quad \rho_4<0, \tag{24}$$

which decays as $|z|\to\infty$ and therefore generates localized (bright) envelopes in Eq. (20).

(II) Singular soliton:

$$f(z)=\left[\pm\sqrt{\frac{\rho_2}{\rho_4}}\operatorname{csch}\left(n\sqrt{\rho_2}z\right)\right]^{\frac{1}{n}},\quad \rho_2>0,\quad \rho_4>0, \tag{25}$$

which is singular at $z=0$ and may generate singular traveling-wave envelopes.

Family 2. If $\rho_1=\rho_3=0$ and $\rho_0=\rho_2^2/4\rho_4$, Eq. (21) supports kink-type solutions with nonzero background:

(I) Dark soliton:

$$f(z)=\left[\pm\sqrt{-\frac{\rho_2}{2\rho_4}}\tanh\left(n\sqrt{\frac{\rho_2}{2}}z\right)\right]^{\frac{1}{n}},\quad \rho_2<0,\quad \rho_4>0, \tag{26}$$

which approaches constants as $|z|\to\infty$ and thus yields dark-type envelopes (intensity dips on a finite pedestal) once substituted into Eq. (20).

(II) Singular soliton:

$$f(z)=\left[\pm\sqrt{-\frac{\rho_2}{2\rho_4}}\coth\left(n\sqrt{-\frac{\rho_2}{2}}z\right)\right]^{\frac{1}{n}},\quad \rho_2\langle 0,\rho_4\rangle 0, \tag{27}$$

which is singular at $z=0$.

Family 3. If $\rho_1 = \rho_3 = 0$, Eq. (21) admits solutions expressed in terms of the Weierstrass elliptic function (WEF), denoted by $\wp(nz;r_2,r_3)$, where r_2 and r_3 are the corresponding Weierstrass invariants. The WEF satisfies the differential equation:

$$(\wp')^2 = 4\wp^3 - r_2\wp - r_3.$$

(I) For the invariants $r_2 = \dfrac{4\rho_2^2 - 12\rho_0\rho_4}{3}$ and $r_3 = \dfrac{4\rho_2\left(-2\rho_2^2 + 9\rho_0\rho_4\right)}{27}$, the following two distinct WEF solution are obtained:

$$f(z) = \left[\frac{1}{\rho_4}\wp(nz,r_2,r_3) - \frac{\rho_2}{3\rho_4}\right]^{\frac{1}{2n}}, \tag{28}$$

and

$$f(z) = \left[\frac{3\rho_0}{3\wp(nz,r_2,r_3) - \rho_2}\right]^{\frac{1}{2n}}. \tag{29}$$

(II) For the invariants $r_2 = \dfrac{\rho_2^2}{12} + \rho_0\rho_4$ and $r_3 = \dfrac{\rho_2\left(36\rho_0\rho_4 - \rho_2^2\right)}{216}$, we have WEF solutions

$$f(z) = \left[\frac{6\sqrt{\rho_0}\,\wp(nz,r_2,r_3) + \rho_2\sqrt{\rho_0}}{3\wp'(nz,r_2,r_3)}\right]^{\frac{1}{n}}, \tag{30}$$

and

$$f(z) = \left[\frac{3\sqrt{\rho_4^{-1}}\,\wp'(nz,r_2,r_3)}{6\wp(nz,r_2,r_3) + \rho_2}\right]^{\frac{1}{n}}, \tag{31}$$

where $\wp'(nz,r_2,r_3) = \dfrac{d}{dz}\wp(nz,r_2,r_3)$.

Eqs. (28)–(29) and Eqs. (30)–(31) each satisfy the same auxiliary equation under the above parameter conditions and constitute two distinct branches of the WEF solution family.

The WEF $\wp(z)$ and the Jacobi elliptic functions provide equivalent representations of elliptic wave solutions. Let u denote the variable of the cubic polynomial

$$4u^3 - r_2u - r_3 = 0,$$

and let e_1, e_2, and e_3 be its three roots. Accordingly, the WEF satisfies

$$(\wp')^2 = 4(\wp - e_1)(\wp - e_2)(\wp - e_3).$$

The parameter k denotes the modulus of the Jacobi elliptic functions and is defined by:

$$k^2 = \frac{e_2 - e_3}{e_1 - e_3},\ 0 \le k \le 1.$$

With these definitions, the WEF are expressed in terms of the Jacobi elliptic function $\mathrm{sn}(\cdot,k)$ as

$$\wp(z) = e_3 + \frac{e_1 - e_3}{\mathrm{sn}^2\left(\sqrt{e_1 - e_3}\,z,k\right)}.$$

Consequently, the WEF solutions in Family 3 may alternatively be rewritten in Jacobi elliptic form. The solitary-wave limits follow from the standard degeneracies of the Jacobi elliptic functions: as $k \to 1$, the solutions reduce to soliton solutions, whereas as $k \to 0$, they reduce to trigonometric periodic waves.

4.1. Soliton solutions

In accordance with the methodology presented above, the balance rule (23) is used to identify the suitable structure of the solution. When applied to Eq. (18), this involves balancing $\phi_1^{(6)}(z)$ against $\phi_1^3(z)$. The resulting dimensional balance yields the following condition:

$$m + 6n = 3m \Rightarrow m = 3n. \tag{32}$$

Upon selecting $n=1$, it follows that $m=3$. This outcome permits the construction of the appropriate solution form for Eq. (18), thereby facilitating the derivation of explicit soliton solutions in terms of the determined parameters m and n. Thus, the solution to Eq. (18) can be written as:

$$\phi_1(z) = \alpha_0 + \alpha_1 f(z) + \alpha_2 f^2(z) + \alpha_3 f^3(z), \tag{33}$$

where $\alpha_0, \alpha_1, \alpha_2$ and α_3 denote constants, subject to the condition $\alpha_3 \neq 0$. Upon substituting (33) and (21) into Eq. (18), the following algebraic equations are obtained:

$$
\begin{aligned}
&41580\alpha_3\rho_4^2\rho_3 = 0,\\
&20160\alpha_3\rho_4^3 + \Delta_4\alpha_3^3 = 0,\\
&720\alpha_1\rho_4^3 + 26730\alpha_3\rho_3^2\rho_4 + 29880\alpha_3\rho_4^2\rho_2 + 3\Delta_4\alpha_1\alpha_3^2 + 360\Delta_1\alpha_3\rho_4^2 = 0,\\[1ex]
&35910\alpha_3\rho_3\rho_4\rho_2 + 540\Delta_1\alpha_3\rho_3\rho_4 + (10395/2)\alpha_3\rho_3^3 + 1260\rho_4^2\alpha_1\rho_3\\
&+3\Delta_4\alpha_0\rho_3^2 + 22680\rho_4^2\alpha_3\rho_1 = 0,\\[1ex]
&408\Delta_1\alpha_3\rho_2\rho_4 + 189\Delta_1\alpha_3\rho_3^2 + 12\Delta_2\alpha_3\rho_4 + 3\Delta_4\alpha_1^2\alpha_3 + 18144\rho_4^2\alpha_3\alpha_0\\
&+25704\rho_4\alpha_3\rho_1\rho_3 + 24\Delta_1\alpha_1\rho_4^2 + 9450\alpha_3\rho_3^2\rho_{42} + 11172\rho_4\alpha_3\rho_2^2\\
&+840\rho_4^2\alpha_1\rho_2 + 630\rho_4\alpha_1\rho_3^2 = 0, \qquad\qquad (34)\\[1ex]
&14805\rho_4\alpha_3\rho_1\rho_2 + 19656\rho_4\rho_3\alpha_3\rho_0 + 630\alpha_1\rho_4^2\rho_1 + (24759/4)\alpha_3\rho_3^2\rho_1\\
&+315\Delta_1\alpha_3\rho_1\rho_4 + \frac{315}{4}\alpha_1\rho_3^3 + 30\Delta_1\alpha_1\rho_3\rho_4 + 735\rho_4\alpha_1\rho_2\rho_3 + \frac{21}{2}\Delta_2\alpha_3\rho_3\\
&+6\Delta_4\alpha_0\alpha_1\alpha_3 + \frac{525}{2}\Delta_1\alpha_3\rho_2\rho_3 + \frac{10101}{2}\alpha_3\rho_2^2\rho_3 = 0,\\[1ex]
&\frac{45}{4}\alpha_3\rho_1^3 + \frac{1}{2}\alpha_1\rho_2^2\rho_1 + \Delta_4\alpha_0^3 + 15\rho_3\alpha_1\rho_0\rho_2 + \frac{1}{2}\Delta_1\alpha_1\rho_2\rho_1 + 18\Delta_1\alpha_3\rho_0\rho_1\\
&+3\Delta_1\alpha_1\rho_3\rho_0 + \frac{9}{4}\rho_3\alpha_1\rho_1^2 + 270\rho_3\alpha_3\rho_0^2 + \frac{1}{2}\Delta_2\alpha_1\rho_1 + \Delta_3\alpha_0 + 36\alpha_1\rho_0\rho_4\rho_1\\
&+225\alpha_3\rho_0\rho_2\rho_1 = 0,
\end{aligned}
$$

continued on next page

$$\frac{195}{2}\Delta_1\alpha_3\rho_1\rho_2+210\rho_4\alpha_1\rho_2\rho_1+3\Delta_4\alpha_0\alpha_1^2+5670\rho_4\alpha_3\rho_0\rho_1+135\Delta_1\rho_3\alpha_3\rho_0$$
$$+3780\rho_3\alpha_3\rho_0\rho_2+378\rho_4\alpha_1\rho_3\rho_0+\frac{15}{2}\Delta_2\alpha_3\rho_1+15\Delta_1\alpha_1\rho_4\rho_1+\frac{1995}{2}\alpha_3\rho_2^2\rho_1$$
$$+\frac{15}{2}\Delta_1\alpha_1\rho_2\rho_3+\frac{63}{2}\rho_3\alpha_1\rho_2^2+\frac{3}{2}\Delta_2\alpha_1\rho_3+\frac{2835}{2}\rho_3\alpha_3\rho_1^2+63\alpha_1\rho_3^2\rho_1=0,$$

$$\Delta_3\alpha_1+3\Delta_4\alpha_0^2\alpha_1+\Delta_2\alpha_1\rho_2+1512\rho_4\alpha_3\rho_0^2+1512\rho_3\alpha_3\rho_0\rho_1+\alpha_1\rho_2^3+\Delta_1\alpha_1\rho_2^2$$
$$+315\alpha_3\rho_1^2\rho_2+45\rho_4\alpha_1\rho_1^2+27\rho_3\alpha_1\rho_2\rho_1+\frac{9}{2}\Delta_1\alpha_1\rho_1\rho_3+546\alpha_3\rho_0\rho_2^2+\frac{45}{2}\Delta_1\alpha_3\rho_1^2 \quad (34)$$
$$+60\Delta_1\alpha_3\rho_0\rho_2+12\Delta_1\alpha_1\rho_0\rho_4+6\Delta_2\alpha_3 ?_0+45\alpha_1\rho_3^2\rho_0+132\rho_4\alpha_1\rho_0\rho_2=0,$$

$$20\Delta_1\alpha_1\rho_2\rho_4+105\rho_3^2\alpha_1\rho_2+3\Delta_4\alpha_0^2\alpha_3+4455\rho_4\alpha_3\rho_1^2+182\rho_4\alpha_1\rho_2^2+504\rho_4\alpha_1\rho_1\rho_3$$
$$+9\Delta_2\alpha_3\rho_2+\frac{369}{2}\Delta_1\alpha_3\rho_1\rho_3+81\Delta_1\alpha_3\rho_2^2+729\alpha_3\rho_2^3+4455\rho_3^2\alpha_3\rho_0+252\Delta_1\alpha_3\rho_0\rho_4$$
$$+2\Delta_2\alpha_1\rho_4+\Delta_4\alpha_1^3+(15/2)\Delta_1\alpha_1\rho_3^2+\Delta_3\alpha_3+10548\rho_4\alpha_3\rho_0\rho_2+504\alpha_1\rho_0\rho_4^2$$
$$+5823\alpha_3\rho_2\rho_3\rho_1=0.$$

Set-1: By imposing the auxiliary parameter constraints $\rho=\rho_0=\rho_1=\rho=0$, the algebraic system (34) reduces to an integrable form corresponding to the first family of the sub-ODE. These constraints are mathematical conditions on the auxiliary equation rather than direct restrictions on the physical parameters of the optical model. Solving the resulting algebraic system yields the following solution results.

Result-1:

$$\begin{aligned}&\alpha_0=0, \qquad \alpha_1=\frac{288}{581}\Delta_1\sqrt{-\frac{35\rho_4}{\Delta_4}},\\ &\alpha_2=0, \qquad \alpha_3=24\rho_4\sqrt{-\frac{35\rho_4}{\Delta_4}},\\ &\rho_2=\frac{17}{581}\Delta_1,\end{aligned} \tag{35}$$

and

$$\Delta_2=\frac{1891}{6889}\Delta_1^2, \Delta_3=-\frac{1748025}{196122941}\Delta_1^3, \tag{36}$$

provided $\Delta_4\rho_4<0$. Upon substituting Eq. (35) together with the solutions (24) and (25) into Eq. (33), one arrives at the following solutions for Eqs. (1) and (2):

(I) Bright soliton solutions:

$$\begin{aligned}Q(x,t)&=\pm\frac{408\Delta_1}{581}\sqrt{\frac{85\Delta_1}{83\Delta_4}}\operatorname{sech}\left(\sqrt{\frac{17\Delta_1}{581}}(x-vt)\right)\left[\operatorname{sech}^2\left(\sqrt{\frac{17\Delta_1}{581}}(x-vt)\right)-\frac{12}{17}\right]\\ &\times\exp\left[i\left(-\kappa x+\omega t+\sigma W-\sigma^2 t\right)\right],\\ R(x,t)&=\pm\frac{408C\Delta_1}{581}\sqrt{\frac{85\Delta_1}{83\Delta_4}}\operatorname{sech}\left(\sqrt{\frac{17\Delta_1}{581}}(x-vt)\right)\left[\operatorname{sech}^2\left(\sqrt{\frac{17\Delta_1}{581}}(x-vt)\right)-\frac{12}{17}\right]\\ &\times\exp\left[i\left(-\kappa x+\omega t+\sigma W-\sigma^2 t\right)\right],\end{aligned} \tag{37}$$

provided $\Delta_1>0$ and $\Delta_4>0$.

(II) Singular soliton solutions:

$$\begin{aligned} Q(x,t) &= \pm\frac{408\Delta_1}{581}\sqrt{-\frac{85\Delta_1}{83\Delta_4}}\operatorname{csch}\left(\sqrt{\frac{17\Delta_1}{581}}(x-vt)\right)\left[\operatorname{sech}^2\left(\sqrt{\frac{17\Delta_1}{581}}(x-vt)\right)+\frac{12}{17}\right] \\ &\quad\times\exp\left[i\left(-\kappa x+\omega t+\sigma W-\sigma^2 t\right)\right], \\ R(x,t) &= \pm\frac{408C\Delta_1}{581}\sqrt{-\frac{85\Delta_1}{83\Delta_4}}\operatorname{csch}\left(\sqrt{\frac{17\Delta_1}{581}}(x-vt)\right)\left[\operatorname{sech}^2\left(\sqrt{\frac{17\Delta_1}{581}}(x-vt)\right)+\frac{12}{17}\right] \\ &\quad\times\exp\left[i\left(-\kappa x+\omega t+\sigma W-\sigma^2 t\right)\right], \end{aligned} \tag{38}$$

provided $\Delta_1 > 0$ and $\Delta_4 < 0$.

Result-2:

$$\begin{aligned} &\alpha_0 = 0, \quad \alpha_1 = 0, \\ &\alpha_2 = 0, \quad \alpha_3 = 24, \\ &\rho_4\sqrt{-\frac{35\rho_4}{\Delta_4}}, \quad \rho_2 = -\frac{\Delta_1}{83}, \end{aligned} \tag{39}$$

and

$$\Delta_2 = \frac{1891\Delta_1^2}{6889}, \quad \Delta_3 = \frac{11025\Delta_1^3}{571787}, \tag{40}$$

provided $\Delta_4\rho_4 < 0$. Upon substituting Eq. (39) together with the solutions (24) and (25) into Eq. (33), one arrives at the following solutions for Eqs. (1) and (2):

(I) Bright soliton solutions:

$$\begin{aligned} Q(x,t) &= \pm\frac{24\Delta_1}{6889}\sqrt{-\frac{2905\Delta_1}{\Delta_4}}\operatorname{sech}^3\left(\sqrt{-\frac{\Delta_1}{83}}(x-vt)\right)\exp\left[i\left(-\kappa x+\omega t+\sigma W-\sigma^2 t\right)\right], \\ R(x,t) &= \pm\frac{24C\Delta_1}{6889}\sqrt{-\frac{2905\Delta_1}{\Delta_4}}\operatorname{sech}^3\left(\sqrt{-\frac{\Delta_1}{83}}(x-vt)\right)\exp\left[i\left(-\kappa x+\omega t+\sigma W-\sigma^2 t\right)\right], \end{aligned} \tag{41}$$

provided $\Delta_1 < 0$ and $\Delta_4 > 0$.

(II) Singular soliton solutions:

$$\begin{aligned} Q(x,t) &= \pm\frac{24\Delta_1}{6889}\sqrt{\frac{2905\Delta_1}{\Delta_4}}\operatorname{csch}^3\left(\sqrt{-\frac{\Delta_1}{83}}(x-vt)\right)\exp\left[i\left(-\kappa x+\omega t+\sigma W-\sigma^2 t\right)\right], \\ R(x,t) &= \pm\frac{24C\Delta_1}{6889}\sqrt{\frac{2905\Delta_1}{\Delta_4}}\operatorname{csch}^3\left(\sqrt{-\frac{\Delta_1}{83}}(x-vt)\right)\exp\left[i\left(-\kappa x+\omega t+\sigma W-\sigma^2 t\right)\right], \end{aligned} \tag{42}$$

Set-2: Set $\rho_1 = \rho_3 = 0, \rho_0 = \frac{\rho_2^2}{4\rho_4}$ in Eqs. (34) and solve it, one gets the following result:

$$\begin{aligned} &\alpha_0 = 0, \qquad \alpha_1 = \frac{18\Delta_1}{83}\sqrt{-\frac{35\rho_4}{\Delta_4}}, \\ &\alpha_2 = 0, \qquad \alpha_3 = 24\rho_4\sqrt{-\frac{35\rho_4}{\Delta_4}}, \qquad \rho_2 = \frac{\Delta_1}{166}, \end{aligned} \tag{43}$$

and

$$\Delta_2 = \frac{946\Delta_1^2}{6889}, \qquad \Delta_3 = -\frac{1260\Delta_1^3}{571787}, \tag{44}$$

provided $\Delta_4\rho_4 < 0$. Upon substituting Eq. (43) together with the solutions (26) and (27) into

Eq. (33), one arrives at the following solutions for Eqs. (1) and (2):

(I) Dark soliton solutions:

$$\begin{aligned} Q(x,t) &= \pm\frac{3\Delta_1}{6889}\sqrt{\frac{2905\Delta_1}{\Delta_4}}\tanh\left(\frac{1}{2}\sqrt{-\frac{\Delta_1}{83}}(x-vt)\right) \\ &\times\left[\tanh^2\left(\frac{1}{2}\sqrt{-\frac{\Delta_1}{83}}(x-vt)\right)-3\right] \\ &\times\exp\left[i\left(-\kappa x+\omega t+\sigma W-\sigma^2 t\right)\right], \\ R(x,t) &= \pm\frac{3C\Delta_1}{6889}\sqrt{\frac{2905\Delta_1}{\Delta_4}}\tanh\left(\frac{1}{2}\sqrt{-\frac{\Delta_1}{83}}(x-vt)\right) \\ &\times\left[\tanh^2\left(\frac{1}{2}\sqrt{-\frac{\Delta_1}{83}}(x-vt)\right)-3\right] \\ &\times\exp\left[i\left(-\kappa x+\omega t+\sigma W-\sigma^2 t\right)\right]. \end{aligned} \tag{45}$$

(II) Singular soliton solutions:

$$\begin{aligned} Q(x,t) &= \pm\frac{3\Delta_1}{6889}\sqrt{\frac{2905\Delta_1}{\Delta_4}}\coth\left(\frac{1}{2}\sqrt{-\frac{\Delta_1}{83}}(x-vt)\right) \\ &\times\left[\coth^2\left(\frac{1}{2}\sqrt{-\frac{\Delta_1}{83}}(x-vt)\right)-3\right] \\ &\times\exp\left[i\left(-\kappa x+\omega t+\sigma W-\sigma^2 t\right)\right], \\ R(x,t) &= \pm\frac{3C\Delta_1}{6889}\sqrt{\frac{2905\Delta_1}{\Delta_4}}\coth\left(\frac{1}{2}\sqrt{-\frac{\Delta_1}{83}}(x-vt)\right) \\ &\times\left[\coth^2\left(\frac{1}{2}\sqrt{-\frac{\Delta_1}{83}}(x-vt)\right)-3\right] \\ &\times\exp\left[i\left(-\kappa x+\omega t+\sigma W-\sigma^2 t\right)\right], \end{aligned} \tag{46}$$

provided that $\Delta_1 < 0$ and $\Delta_4 < 0$, which are the same parameter conditions required for Eq. (45).

Set-3: Set $\rho_1 = \rho_3 = 0$ in Eqs. (34) and solve it, one gets the following result:

$$\begin{aligned} &\alpha_0 = 0, \qquad \alpha_1 = 0, \qquad \alpha_2 = 0, \qquad \alpha_3 = 24\rho_4\sqrt{-\frac{35\rho_4}{\Delta_4}}, \\ &\rho_0 = \frac{32\Delta_1^2}{241115\rho_4}, \qquad \rho_2 = -\frac{\Delta_1}{83}, \end{aligned} \tag{47}$$

and

$$\begin{aligned} \Delta_2 &= \frac{2543\Delta_1^2}{34445}, \\ \Delta_3 &= -\frac{381357\Delta_1^3}{20012545}, \end{aligned} \tag{48}$$

subject to $\rho_4\Delta_4 < 0$, $\rho_4 \neq 0$, $\Delta_4 \neq 0$. Substituting Eq. (47), together with Eqs. (28)–(31), into Eq. (33) yields the following WEF solutions of Eqs. (1) and (2):

(I)

$$Q(x,t)=\pm\frac{24\sqrt{-35\Delta_4}}{\Delta_4}\left[\wp\left((x-vt),-\frac{244\Delta_1^2}{723345},-\frac{872\Delta_1^3}{540338715}\right)+\frac{\Delta_1}{249}\right]^{\frac{3}{2}}$$
$$\times\exp\left[i\left(-\kappa x+\omega t+\sigma W-\sigma^2 t\right)\right],$$
$$R(x,t)=\pm\frac{24C\sqrt{-35\Delta_4}}{\Delta_4}\left[\wp\left((x-vt),-\frac{244\Delta_1^2}{723345},-\frac{872\Delta_1^3}{540338715}\right)+\frac{\Delta_1}{249}\right]^{\frac{3}{2}}$$
$$\times\exp\left[i\left(-\kappa x+\omega t+\sigma W-\sigma^2 t\right)\right]. \tag{49}$$

(II)

$$Q(x,t)=\pm\frac{9216\sqrt{-6\Delta_4}}{20012545\Delta_4}\left[\frac{\Delta_1^2}{3\wp\left((x-vt),-\frac{244\Delta_1^2}{723345},-\frac{872\Delta_1^3}{540338715}\right)+\frac{\Delta_1}{83}}\right]^{\frac{3}{2}}$$
$$\times\exp\left[i\left(-\kappa x+\omega t+\sigma W-\sigma^2 t\right)\right],$$
$$R(x,t)=\pm\frac{9216C\sqrt{-6\Delta_4}}{20012545\Delta_4}\left[\frac{\Delta_1^2}{3\wp\left((x-vt),-\frac{244\Delta_1^2}{723345},-\frac{872\Delta_1^3}{540338715}\right)+\frac{\Delta_1}{83}}\right]^{\frac{3}{2}}$$
$$\times\exp\left[i\left(-\kappa x+\omega t+\sigma W-\sigma^2 t\right)\right]. \tag{50}$$

(III)

$$Q(x,t)=\pm\frac{1024\Delta_1^3\sqrt{-2\Delta_4}}{180112905\Delta_4}\left[\frac{498\wp\left((x-vt),\frac{419\Delta_1^2}{2893380},-\frac{1117/\Delta_1^3}{4322709720}\right)-\Delta_1}{83\wp'\left((x-vt),\frac{419\Delta_1^2}{2893380},-\frac{1117/\Delta_1^3}{4322709720}\right)}\right]^3$$
$$\times\exp\left[i\left(-\kappa x+\omega t+\sigma W-\sigma^2 t\right)\right],$$
$$R(x,t)=\pm\frac{1024C\Delta_1^3\sqrt{-2\Delta_4}}{180112905\Delta_4}\left[\frac{498\wp\left((x-vt),\frac{419\Delta_1^2}{2893380},-\frac{1117/\Delta_1^3}{4322709720}\right)-\Delta_1}{83\wp'\left((x-vt),\frac{419\Delta_1^2}{2893380},-\frac{1117/\Delta_1^3}{4322709720}\right)}\right]^3$$
$$\times\exp\left[i\left(-\kappa x+\omega t+\sigma W-\sigma^2 t\right)\right]. \tag{51}$$

(IV)

$$Q(x,t)=\pm\frac{648\sqrt{-35\Delta_4}}{\Delta_4}\left[\frac{83\wp'\left((x-vt),\frac{419\Delta_1^2}{2893380},-\frac{1117/\Delta_1^3}{4322709720}\right)}{498\wp\left((x-vt),\frac{419\Delta_1^2}{2893380},-\frac{1117/\Delta_1^3}{4322709720}\right)-\Delta_1}\right]^3$$
$$\times\exp\left[i\left(-\kappa x+\omega t+\sigma W-\sigma^2 t\right)\right],$$
$$R(x,t)=\pm\frac{648C\sqrt{-35\Delta_4}}{\Delta_4}\left[\frac{83\wp'\left((x-vt),\frac{419\Delta_1^2}{2893380},-\frac{1117/\Delta_1^3}{4322709720}\right)}{498\wp\left((x-vt),\frac{419\Delta_1^2}{2893380},-\frac{1117/\Delta_1^3}{4322709720}\right)-\Delta_1}\right]^3$$
$$\times\exp\left[i\left(-\kappa x+\omega t+\sigma W-\sigma^2 t\right)\right]. \tag{52}$$

5. Physical interpretation of soliton solutions

Soliton solutions are central to nonlinear science because they capture stable, localized wave structures that arise from an exact balance between dispersive spreading and nonlinear self-focusing or self-defocusing effects. Depending on their mathematical form, these solutions may describe bright solitons, which appear as localized pulses on a zero background, or dark solitons, which manifest as localized intensity dips within a continuous wave field. Interpreting the physical significance of these soliton types allows us to understand how different mechanisms-whether deterministic dynamics or stochastic perturbations-influence key characteristics such as amplitude, spatial width, propagation speed, and long-term stability. In the following subsections, we provide a detailed examination and comparison of the physical behavior associated with both bright and dark soliton families, highlighting how their qualitative features emerge from the underlying model parameters and nonlinear interactions.

5.1. Bright soliton solution

The sech-type expression corresponds to a bright soliton, i.e., a localized wave packet with a smooth bellshaped profile that vanishes at large distances. In physical terms, the amplitude specifies the soliton's peak value, the inverse width dictates how tightly it is confined, and the velocity determines its motion in the medium. Moreover, the complex exponential phase introduces an internal oscillatory behavior to the field components. The parameter sets used here are selected to reflect physically attainable dispersion/nonlinearity regimes in real optical fibers over the considered bandwidth, and σ model's realistic levels of random phase fluctuations due to environmental and birefringence-induced perturbations. In this context, the parameters are selected as: $a_{11}=1, a_{12}=0.47571,\ \ a_{13}=1, a_{14}=1.2222, a_{15}=1,\ \ a_{16}=1, \kappa=0.16667,\ \ \ C=2,$ $b_{14}=1$, $b_{15}=1, v=0.78382$ and $W(t)=2t$.

We examine four representative values of noise strength, $\sigma=0,1,5,$ and 10. In all cases, the exact solution retains the same general structure: its modulus is independent of σ, whereas the deterministic component of the effective frequency is shifted according to the Itô correction, such that $\omega_{eff}=\omega-\sigma^2$. Thus, the effective frequency decreases linearly with the noise power σ^2. Consequently, for all noise strengths considered, the envelope $|Q(x,t)|$ represents a bright soliton: the intensity $|Q|^2$ forms a single, strongly localized hump centered at $x=vt$ those decays rapidly as $|x-vt|\to\infty$. The 3D and contour plots of absolute value confirm that the soliton propagates with essentially constant amplitude and width for $\sigma=1,1,5,10$, so the energy carried by the pulse is transported coherently through the medium despite the presence of stochastic forcing. The influence of the noise strength appears primarily in the phase factor.

Figure 1: for $\sigma=0$, $\omega=0.18911$ (deterministic case), the real and imaginary parts describe the in-phase and quadrature components of a coherent carrier wave of moderate frequency trapped inside the soliton envelope. The corresponding 3D and contour plots show relatively smooth oscillations in space and time, fully confined within the bright hump.

Figure 2: when $\sigma=1$, $\omega=1.1891$, the envelope remains unchanged, but the effective frequency increases; hence $\Re Q$ and $\Im Q$ exhibit a denser pattern of oscillations in the (x,t) -plane. The 3D surfaces become more corrugated, the contour plots display finer interference fringes, and the 2D slices reveal more carrier cycles under the same envelope. This illustrates that moderate Itô noise mainly induces additional phase modulation without degrading the intensity profile.

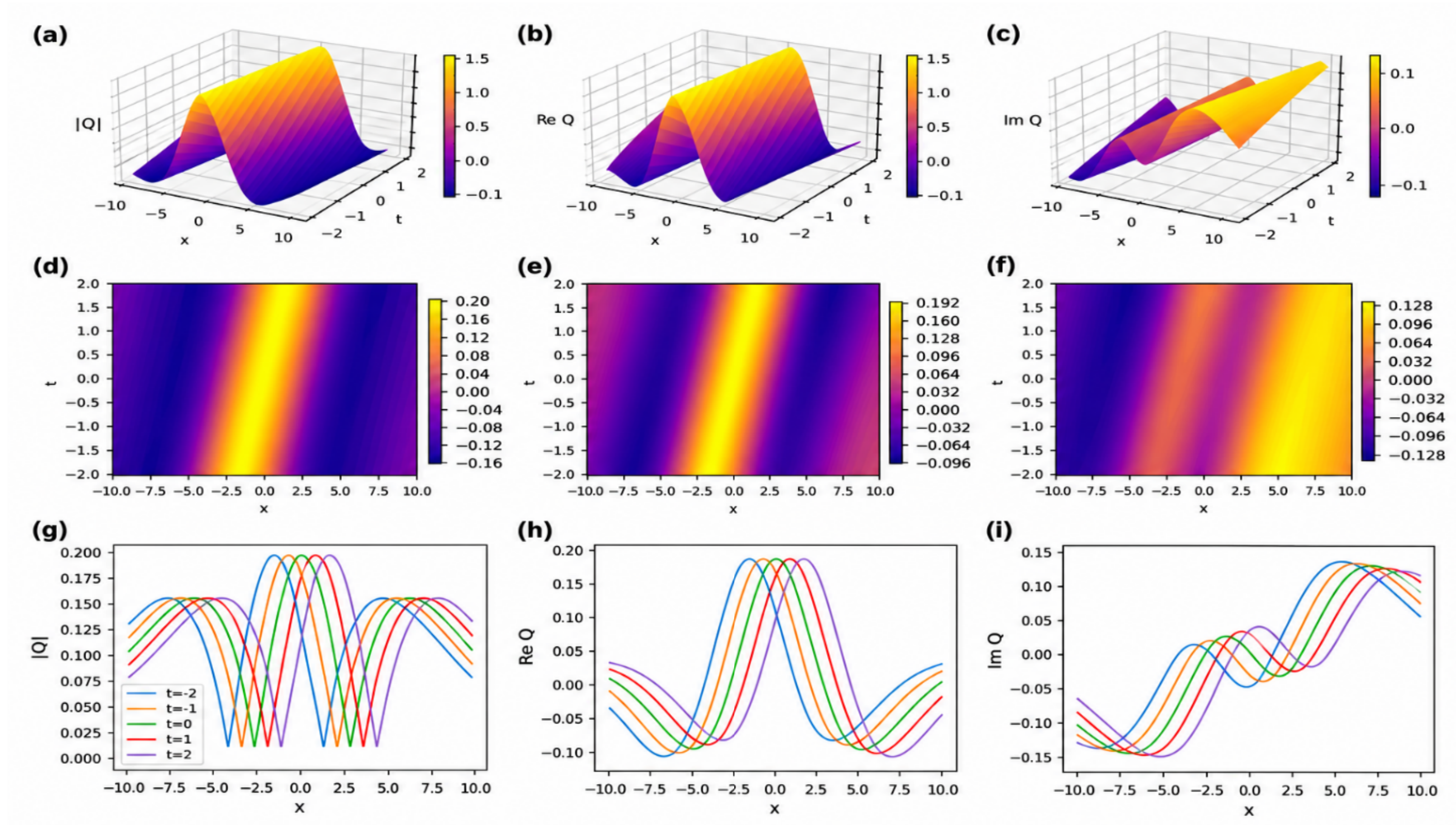

Fig. 1. Bright soliton solution (37) for σ=0. (a)–(c) 3D-plots of |Q|, Re(Q), and Im(Q), respectively. (d)–(f) Corresponding contour plots. (g)–(i) 2D profiles of |Q(x,t)|, Re(Q(x,t)), and Im(Q(x,t)), respectively. In panels (a)–(c), the solution profiles overlap along the z -direction, indicating that the soliton propagates without changes in its amplitude or shape.

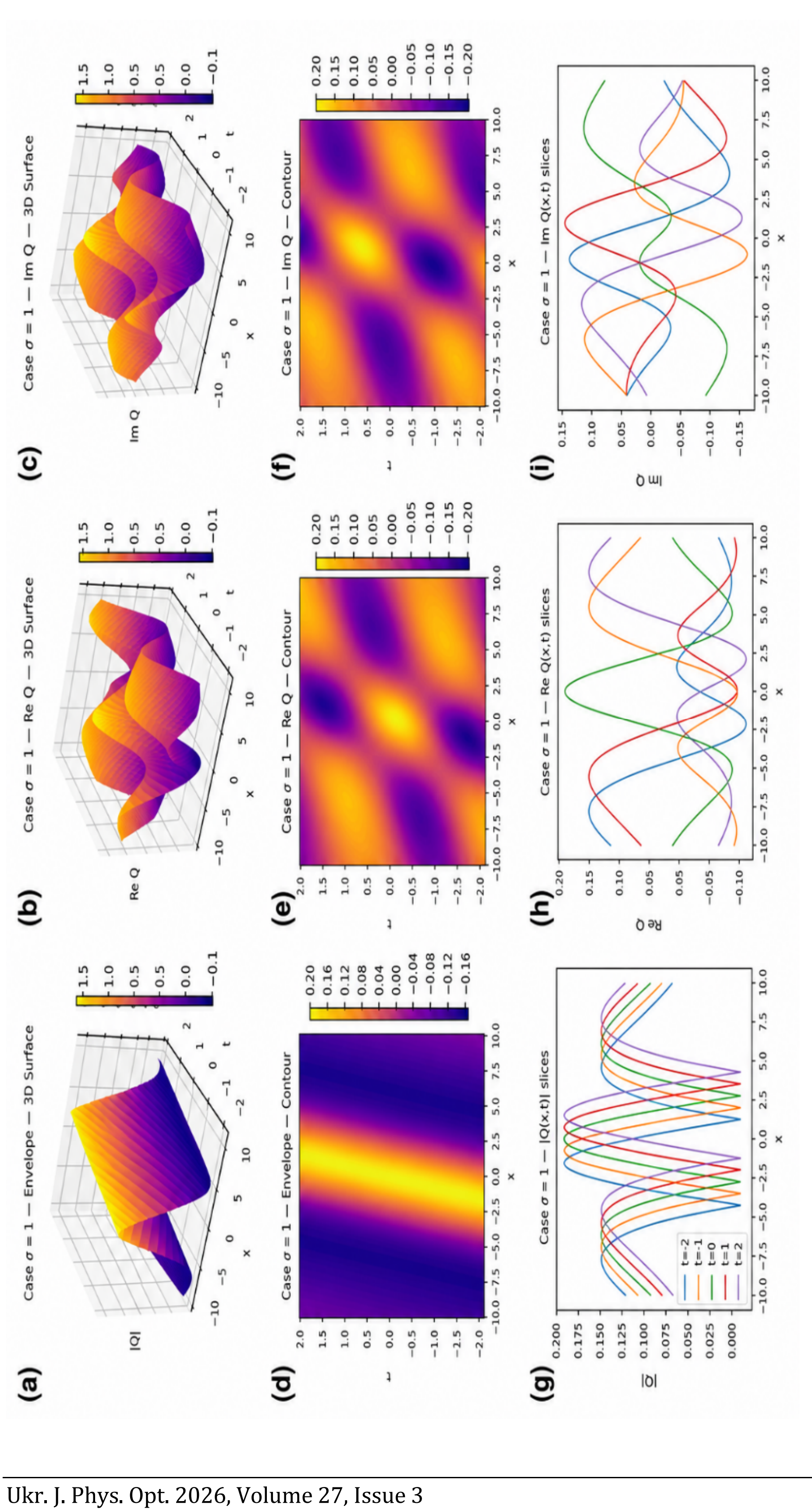

Fig. 2. Bright soliton solution (37) for $\sigma=1$. (a)–(c) 3D-plots of $|Q|$, $\mathrm{Re}(Q)$, and $\mathrm{Im}(Q)$, respectively. (d)–(f) Corresponding contour plots. (g)–(i) 2D profiles of $|Q(x,t)|$, $\mathrm{Re}(Q(x,t))$, and $\mathrm{Im}(Q(x,t))$, respectively. In panels (a)–(c), the solution profiles overlap along the Z-direction, indicating that the soliton propagates with an invariant envelope, while the stochastic perturbation primarily influences the phase of the wave.

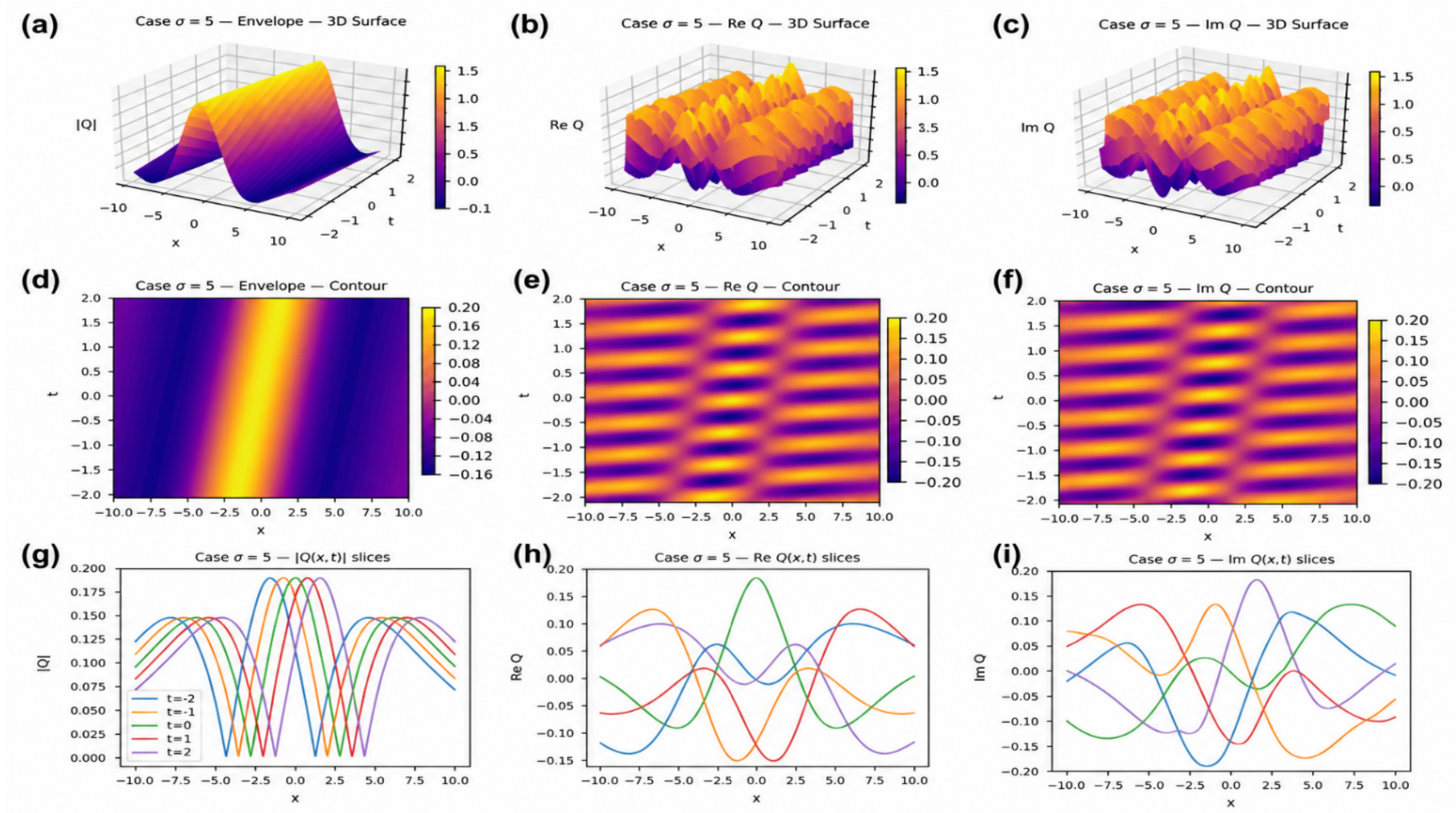

Fig. 3. Bright soliton solution (37) for σ=5. (a)–(c) 3D-plots of |Q|, Re(Q), and Im(Q), respectively. (d)–(f) Corresponding contour plots. (g)–(i) 2D profiles of |Q (x,t)|, Re(Q(x,t)), and Im(Q(x,t)), respectively. In panels (a)–(c), the solution profiles overlap along the Z-direction, confirming that the soliton preserves its envelope during propagation. The increase in the noise strength primarily enhances the stochastic phase modulation without altering the amplitude or width of the soliton.

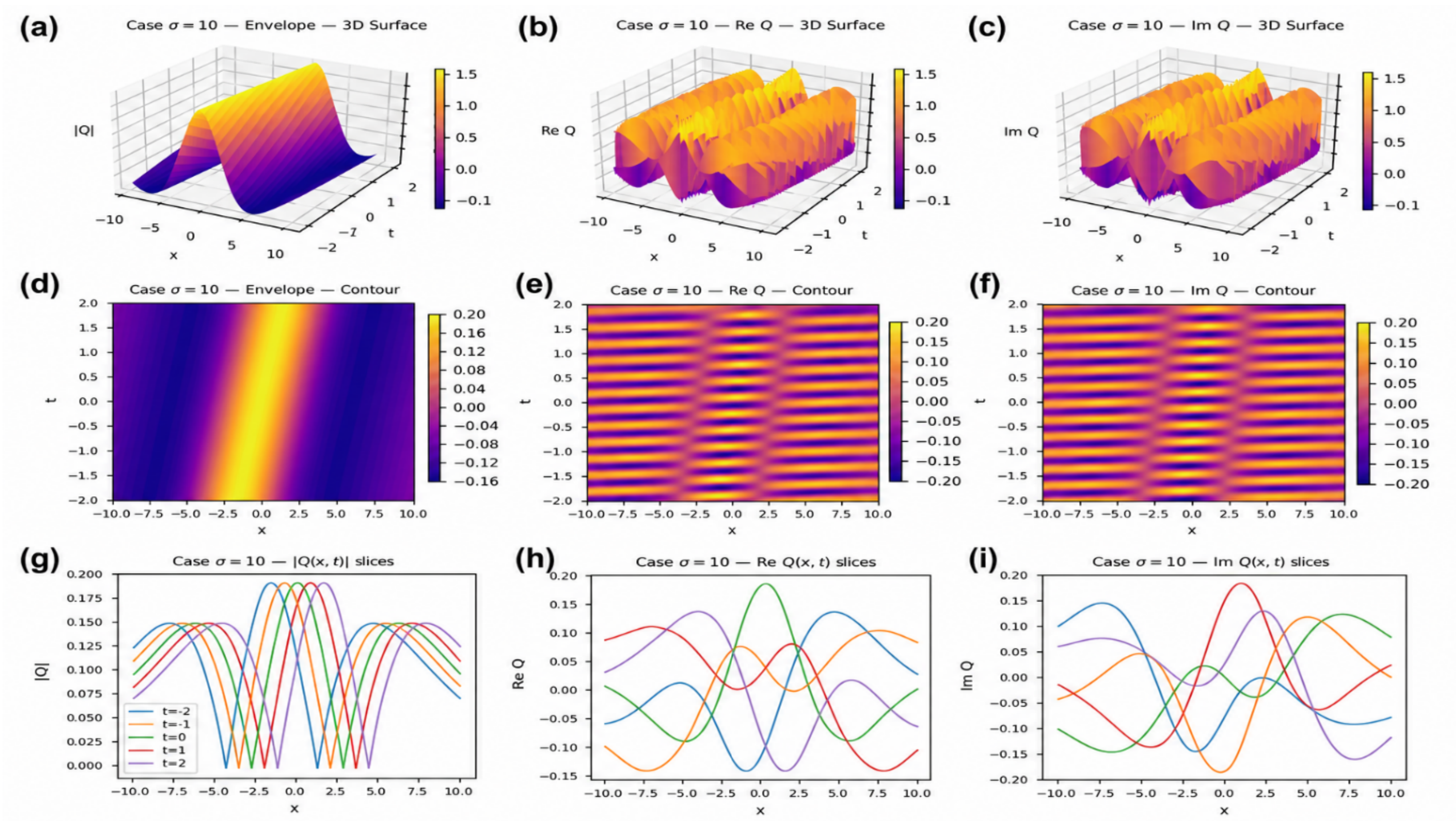

Fig. 4. Bright soliton solution (37) for σ=10. (a)–(c) 3D-plots of |Q|, Re(Q), and Im(Q), respectively. (d)–(f) Corresponding contour plots. (g)–(i) 2D profiles |Q(x,t)|, Re(Q(x,t)), and Im(Q(x,t)), respectively. In panels (a)–(c), the solution profiles overlap along the Z-direction, indicating that the soliton propagates with an invariant envelope despite the increased noise strength, while the influence of the noise is manifested primarily through phase oscillations.

Figure 3: for $\sigma=5,\omega=25.189$, the envelope $\left|Q(x,t)\right|$ is still preserved, but the effective frequency is much larger; as a result, $\Re Q$ and $\Im Q$ present very rapid oscillations in both space and time. In this high-noise regime the soliton behaves as a strongly phase-scrambled but still intensity-localized structure: the pulse energy remains confined, yet its internal phase becomes highly oscillatory and sensitive to stochastic effects.

Figure 4: for $\sigma=10$, the same qualitative trend persists at a higher level. The envelope modulus $\left|Q(x,t)\right|$ remains essentially unchanged (robust amplitude and width), whereas $\Re Q$ and $\Im Q$ develop even denser oscillatory patterns due to stronger stochastic phase modulation. This additional case helps delineate the onset of pronounced phase scrambling without envelope degradation.

These solutions describe bright stochastic solitons of a nonlinear Schrödinger-type medium subject to Itô noise, where $|Q(x,t)|^2$ represents an optical intensity packet and $\Re Q,\Im Q$ encode its coherent quadrature components. The fact that the envelope is almost insensitive to σ while the phase is strongly modified indicates that the underlying balance between dispersion and nonlinearity is robust against substantial random perturbations: noise mainly alters the coherence and carrier dynamics rather than destroying the solitary wave. This behaviour is relevant for a variety of applications, including optical pulse propagation in noisy fibres and fibre Bragg gratings, soliton-based communication systems operating in the presence of amplifier noise, and matter-wave solitons in Bose-Einstein condensates with random potentials. In such settings these analytical solutions provide explicit benchmarks for how stochastic fluctuations affect the phase and coherence of a soliton while leaving its intensity and localization largely intact, which is important both for the design of noise-resilient devices and for the theoretical understanding of stochastic nonlinear wave dynamics.

5.2. Dark soliton solution

For the dark-type solution governed by a tanh profile, we examine how the dark soliton behaves as the stochastic influence increases, using the system parameters $a_{11}=1,a_{12}=-0.74696,a_{13}=1,a_{14}=1.7778$, $a_{15}=1,a_{16}=1,\kappa=0.16667,C=2$, $b_{14}=1,b_{15}=1$, $v=1.1955$ and $W(t)=2t$. We consider four representative stochastic regimes, $\sigma=0,1,5,10$, where σ denotes the Itô noise intensity. Although the soliton modules remains identical across these cases, each regime exhibits distinct internal phase dynamics, reflecting the different levels of stochastic perturbation acting on the system. This envelope has a kink-like, dark structure: instead of forming an isolated bright hump, it produces a localized transition between two background levels. As a result, $|Q(x,t)|^2$ represents a localized intensity dip (or domain wall) that travels with velocity v while connecting two asymptotic states. The 3D surfaces and contour plots for all values of σ show that this dark front propagates essentially rigidly in the (x,t)-plane, with negligible change in amplitude or width, which is the typical behaviour of dark solitons or nonlinear transition fronts in dispersive media. The effect of the noise strength is encoded primarily through the frequency appearing in the phase factor.

Figure 5: for $\sigma = 0, \omega = 0.20653$ (deterministic case), the real and imaginary parts display relatively smooth oscillations in time, confined within the moving dark front: the 3D plots show gently varying surfaces and the contour plots reveal broad fringes.

Figure 6: when $\sigma = 1, \omega = 1.2065$, the envelope remains unchanged, but the effective frequency is larger, so $\Re Q$ and $\Im Q$ exhibit more pronounced temporal modulation; in the contour plots the fringes become denser, and in the 2D slices more oscillation cycles appear across the same spatial profile.

Figure 7: for $\sigma = 5, \omega = 25.207$, the envelope is still preserved, but the corresponding frequency is much higher, leading to very rapid oscillations of the real and imaginary parts in time while the kink-like intensity profile stays almost fixed. Thus, increasing the Itô noise strength mainly produces additional phase scrambling inside the dark structure, without destroying its overall shape or its ability to propagate as a coherent, localized transition layer.

Figure 8: for $\sigma = 10$, the same qualitative trend persists at a higher-noise level. The envelope modulus preserves its kink-like (dark-front) profile with negligible change in amplitude or width, whereas $\Re Q$ and $\Im Q$ exhibit noticeably denser oscillations due to stronger stochastic phase modulation. This additional case further supports that increasing σ primarily enhances phase fluctuations while leaving the soliton modulus robust.

These solutions describe stochastic dark solitons in a noisy nonlinear Schrödinger-type medium. The modulus $|Q(x,t)|^2$ can represent, for example, the optical intensity in a normally dispersive fibre Bragg grating, or the condensate density in a Bose-Einstein condensate, where dark solitons correspond to propagating density dips on a non-zero background. The real and imaginary parts form the in-phase and quadrature components of the complex field and thus encode the local phase of the wave. The fact that the envelope is almost insensitive to σ while the phase becomes increasingly oscillatory shows that the balance between dispersion and nonlinearity is robust against substantial stochastic perturbations: noise primarily degrades phase but not intensity. This behaviour is important in applications such as dark-soliton-based optical switching and signal processing, information transmission in noisy optical networks, and the control of phase defects in matter-wave systems, where one needs solitary structures that remain stable in amplitude while operating in realistically noisy environments.

5.3. Linear stability

We provide an explicit stability argument showing that the Itô stochastic perturbation does not destabilize the soliton modulus. The central point is that the noise is multiplicative and purely phase-like, and can be removed by a stochastic gauge transform, leaving a deterministic envelope problem.

5.3.1. Stochastic gauge transform and reduction to a deterministic amplitude equation. Consider the Itô stochastic field equation (for simplicity we write the Q-equation; the R-equation follows analogously). The stochastic forcing enters as an imaginary multiplicative term of the form

$$dQ = \mathcal{F}[Q,R]dt + i\sigma Q dW(t), \tag{53}$$

where $\mathcal{F}[Q,R]$ denotes the full deterministic drift (dispersion, higher-order derivatives, and Kerr-type nonlinear terms), and $W(t)$ is a standard Wiener process.

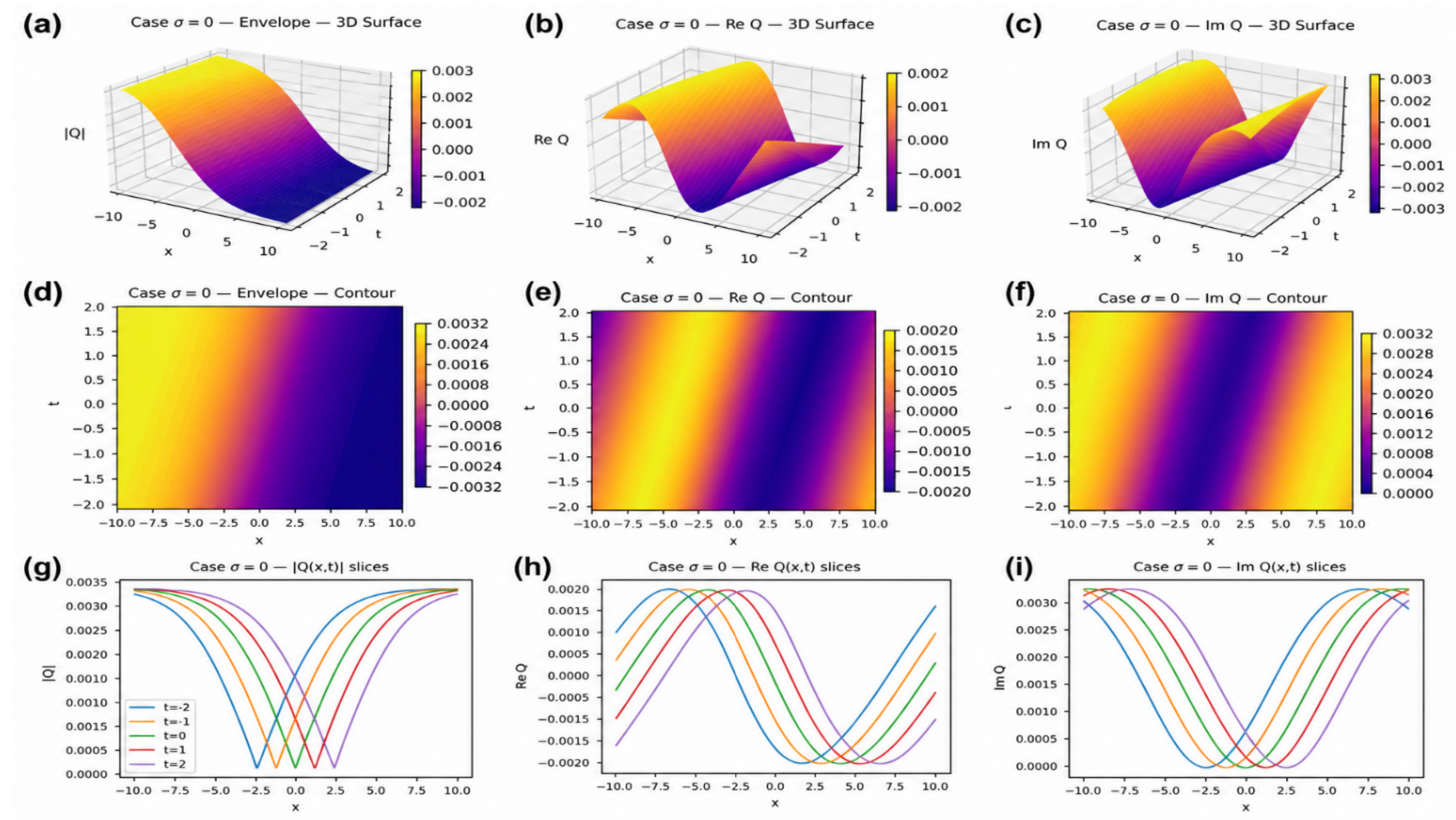

Fig. 5. Dark soliton solution (45) for σ =0. (a)–(c) 3D-plots of |Q|, Re(Q), and Im(Q), respectively. (d)–(f) Corresponding contour plots. (g)–(i) 2D profiles of |Q(x,t)|, Re(Q(x,t)), and Im(Q(x,t)), respectively. In panels (a)–(c), the solution profiles overlap along the Z-direction, demonstrating that the dark soliton propagates with an invariant envelope, while the stochastic perturbation does not affect its amplitude or shape.

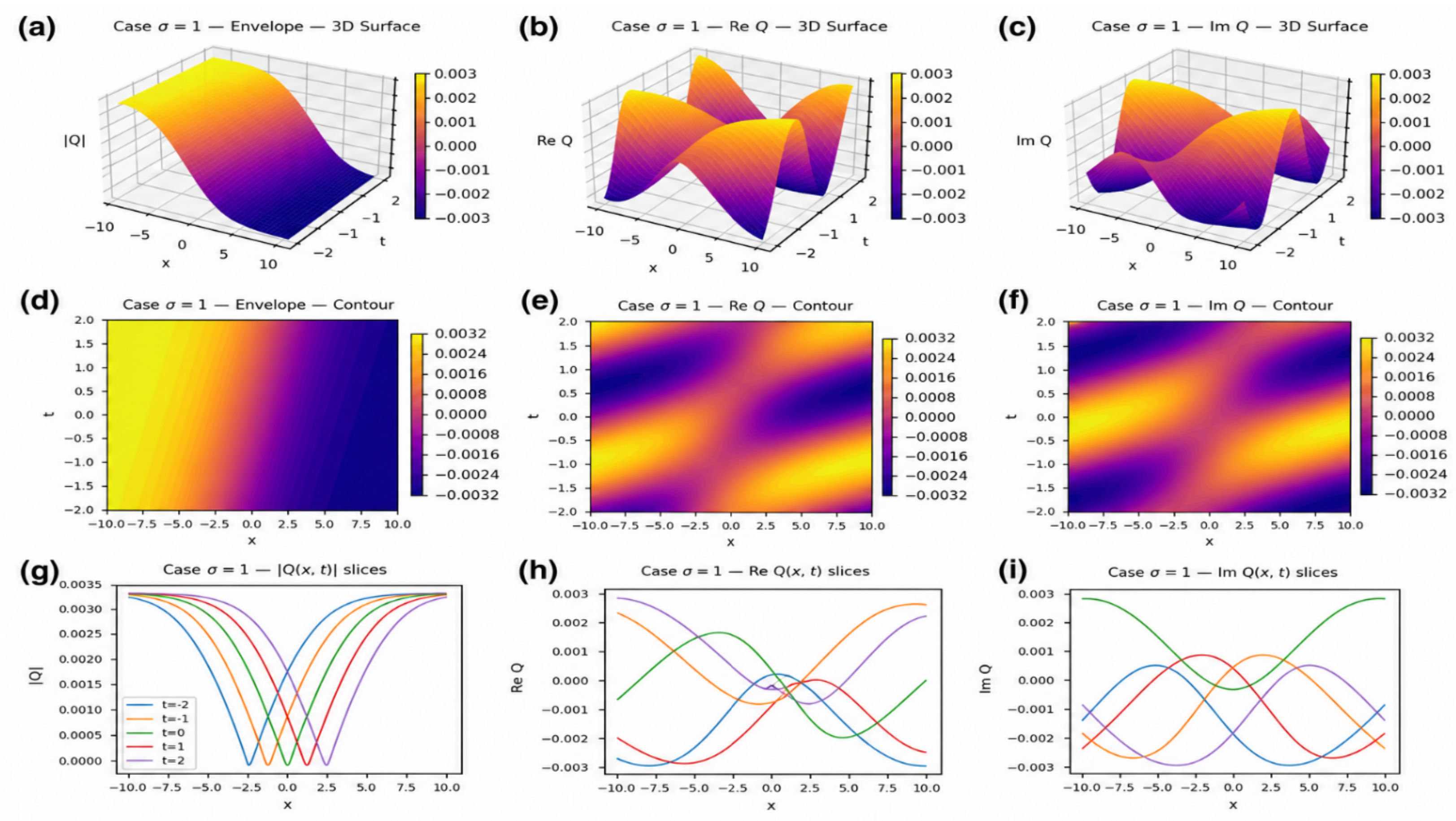

Fig. 6. Dark soliton solution (45) for σ =1. (a)–(c) 3D-plots of of |Q|, Re(Q), and Im(Q), respectively. (d)–(f) Corresponding contour plots. (g)–(i) 2D profiles of |Q(x,t)|, Re(Q(x,t)), and Im(Q(x,t)), respectively. In panels (a)–(c), the solution profiles overlap along the Z-direction, indicating that the dark soliton propagates with an invariant envelope, while the stochastic perturbation primarily affects the phase of the wave.

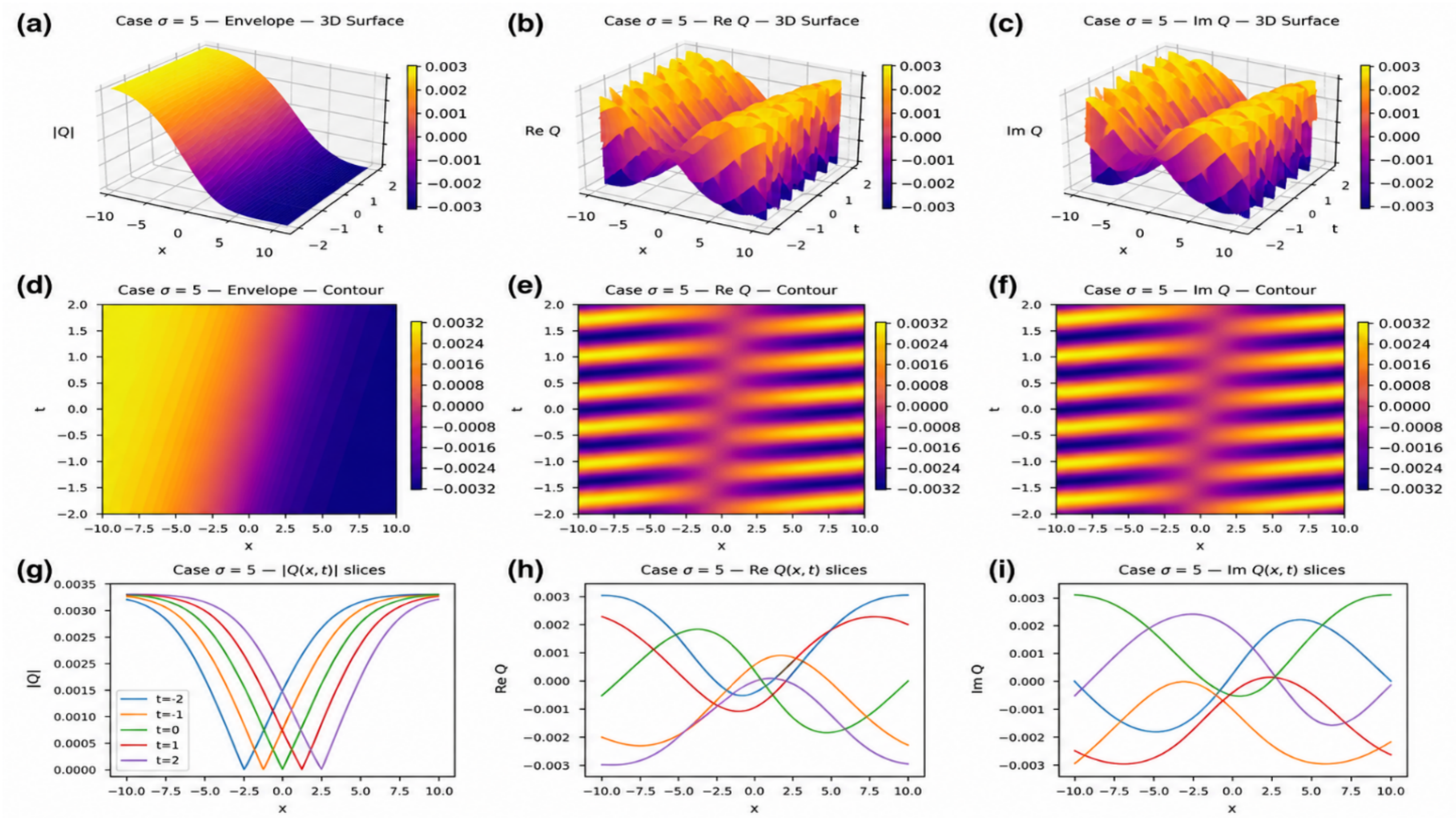

Fig. 7. Dark soliton solution (45) for σ =1. (a)–(c) 3D-plots of |Q|, Re(Q), and Im(Q), respectively. (d)–(f) Corresponding contour plots. (g)–(i) 2D profiles of |Q(x,t)|, Re(Q(x,t)), and Im(Q(x,t)), respectively. In panels (a)–(c), the solution profiles overlap along the Z-direction, confirming that the dark soliton preserves its envelope during propagation. The increase in the noise strength primarily enhances the stochastic phase modulation without affecting the amplitude or width of the soliton.

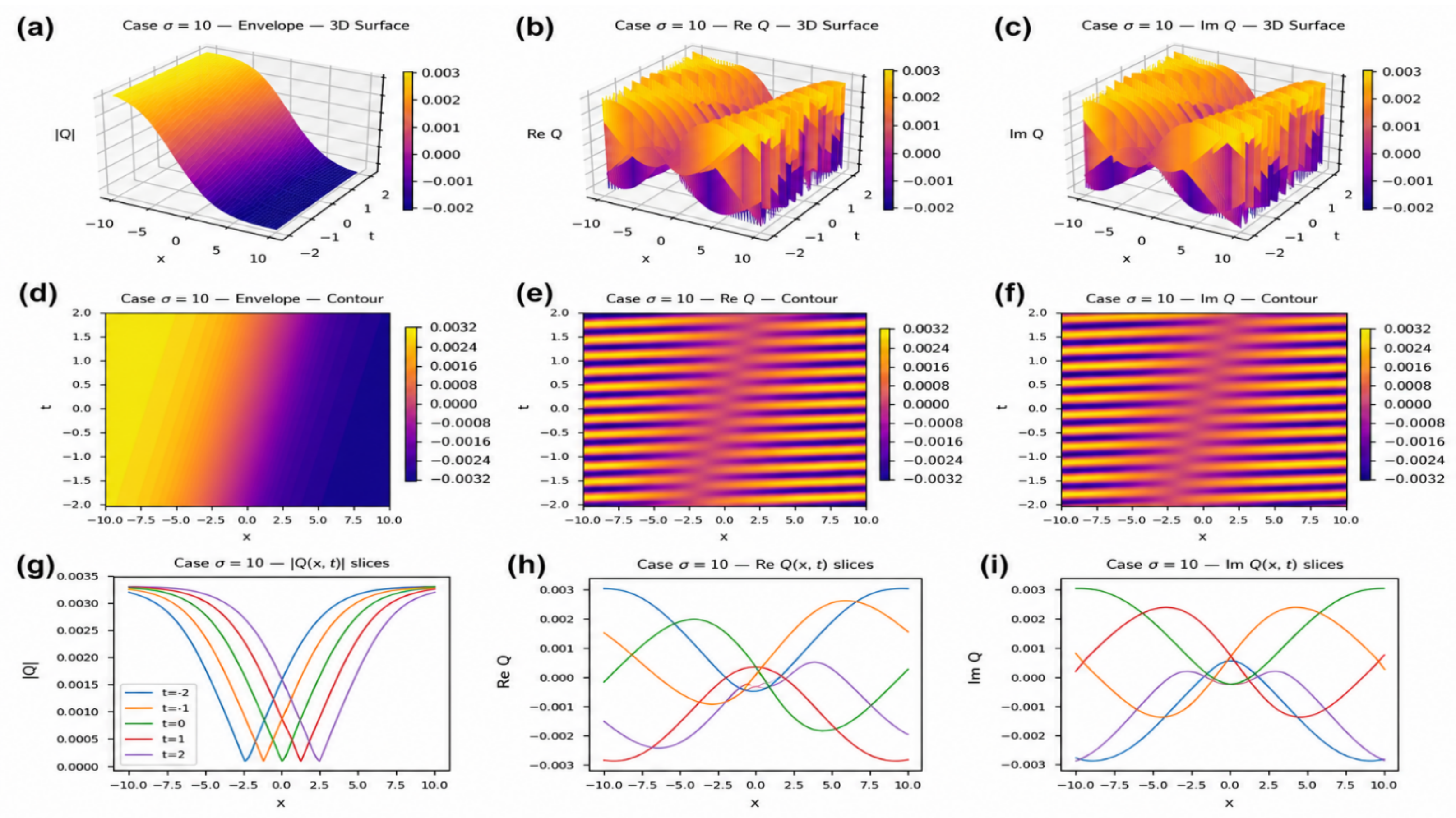

Fig. 8. Dark soliton solution (45) for σ =10. (a)–(c) 3D-plots of |Q|, Re(Q), and Im(Q), respectively. (d)–(f) Corresponding contour plots. (g)–(i) 2D profiles of |Q(x,t)|, Re(Q(x,t)), and Im(Q(x,t)), respectively. In panels (a)–(c), the solution profiles overlap along the Z-direction, showing that the dark soliton preserves its envelope during propagation. Even at σ =10, the stochastic perturbation primarily modifies the phase without changing the soliton amplitude or width of the soliton.

Define the stochastic phase (gauge) factor

$$G(t)=\exp\left(i\sigma W(t)-\frac{1}{2}\sigma^2 t\right), |G(t)|\equiv 1, \tag{54}$$

and introduce the transformed field

$$\tilde{Q}(x,t)=G(t)^{-1}Q(x,t). \tag{55}$$

Using Itô's formula (product rule), one finds

$$d\left(G^{-1}Q\right)=G^{-1}dQ+Qd\left(G^{-1}\right)+dG^{-1},Q. \tag{56}$$

By construction, the $i\sigma QdW$ term in dQ cancels with the $d\left(G^{-1}\right)$ contribution, and the quadratic covariation produces precisely the Itô correction that is absorbed by the factor $-\frac{1}{2}\sigma^2 t$ in (54). As a result, $\tilde{Q}$ satisfies a deterministic evolution equation

$$\partial_t\tilde{Q}=\tilde{\mathcal{F}}\left[\tilde{Q},\tilde{R}\right], \tag{57}$$

with the same spatial/nonlinear structure as the original drift, and with σ appearing only through deterministic parameter shifts (equivalently, through σ^2 in the effective frequency term used in the manuscript). Importantly, since $|G(t)|=1$,

$$|Q(x,t)|\equiv\left|\tilde{Q}(x,t)\right|, \tag{58}$$

so the modulus stability of Q is exactly the modulus stability of $\tilde{Q}$, which is governed by a deterministic equation.

5.3.2. Traveling-wave envelope equation and its linearization. We now consider a traveling-wave solution of the deterministic reduced system in the standard form

$$\tilde{Q}(x,t)=\phi(z)e^{i\Theta(x,t)},\ z=x-vt, \tag{59}$$

where $\phi(z)$ is the real envelope (bright or dark profile) and Θ is a deterministic carrier phase. Substituting (59) into (57) yields the envelope ODE reported in the manuscript,

$$\phi^{(6)}+\Delta_1\phi^{(4)}+\Delta_2\phi''+\Delta_3\phi+\Delta_4\phi^3=0, \tag{60}$$

with deterministic coefficients Δ_j (note that Δ_3 depends on σ^2 through the effective frequency but does not depend on any Wiener realization).

To study robustness of the modulus, perturb only the real envelope:

$$\phi(z)\mapsto\phi(z)+\eta(z,t), |\eta|\ll 1. \tag{61}$$

Linearizing (60) about ϕ gives the linear amplitude (modulus) equation

$$\begin{aligned}&\eta_t=\mathcal{L}\eta\left(\text{ in a co-moving frame}\right),\\&\mathcal{L}:=\partial_z^6+\Delta_1\partial_z^4+\Delta_2\partial_z^2+\left(\Delta_3+3\Delta_4\phi^2(z)\right).\end{aligned} \tag{62}$$

Equivalently, for normal modes $\eta(z,t)=e^{\lambda t}\psi(z)$ we obtain the spectral problem

$$\mathcal{L}\psi=\lambda\psi. \tag{63}$$

This is the explicit linear stability problem for the envelope modulus. Crucially, (63) contains no stochastic forcing and no Wiener path dependence; hence the amplitude channel cannot exhibit trajectory-dependent growth due to the Itô noise.

5.3.3. Neutral mode and spectral stability criterion. Because (60) is translation-invariant in z, differentiation yields

$$\mathcal{L}\phi'(z)=0, \tag{64}$$

so $\lambda=0$ is a neutral eigenvalue corresponding to shifts of the soliton center. Linear modulus stability is obtained if the spectrum of $\mathcal{L}$ satisfies

$$\operatorname{spec}(\mathcal{L})\subset(-\infty,0] \tag{65}$$

with a simple eigenvalue at $\lambda=0$ only due to translation.

Under (65), any sufficiently small amplitude perturbation remains bounded (and typically decays in the co-moving frame), implying stability of the envelope modulus.

5.3.4. Energy (Lyapunov) structure for the envelope and positivity of the second variation. Eq. (60) can be written as an Euler-Lagrange equation for the functional

$$\mathcal{E}[\phi]=\int_{\mathbb{R}}\left[\frac{1}{2}\left(\phi^{(3)}\right)^2-\frac{\Delta_1}{2}\left(\phi''\right)^2+\frac{\Delta_2}{2}\left(\phi'\right)^2+\frac{\Delta_3}{2}\phi^2+\frac{\Delta_4}{4}\phi^4\right]dz, \tag{66}$$

since $\delta\mathcal{E}/\delta\phi=0$ yields (60). The second variation at the soliton profile ϕ is

$$\delta^2\mathcal{E}[\phi](\eta,\eta)=\int_{\mathbb{R}}\left[\begin{array}{l}\left(\eta^{(3)}\right)^2-\Delta_1\left(\eta''\right)^2+\Delta_2\left(\eta'\right)^2\\ +\left(\Delta_3+3\Delta_4\phi^2(z)\right)\eta^2\end{array}\right]dz=\eta,\mathcal{L}\eta. \tag{67}$$

Thus, positivity of $\delta^2\mathcal{E}$ on the subspace orthogonal to the translation mode (i.e., $\eta,\phi'=0$) implies the spectral condition (65) and therefore linear stability of the modulus. Importantly, the stochastic perturbation does not enter (66) or (67) except through deterministic parameter dependence (via σ^2 in Δ_3), hence no noise trajectory can destabilize the amplitude channel.

5.3.5. Interpretation. The above shows that Itô multiplicative noise produces phase diffusion through the gauge factor $G(t)$, while the modulus is controlled by a deterministic self-adjoint linear operator $\mathcal{L}$. Consequently, stability of the envelope modulus is determined by the deterministic spectral/energy properties of (60), and stochasticity primarily degrades coherence (phase) rather than amplitude localization, in agreement with the Monte-Carlo simulations.

6. Conclusions

This study has developed a rigorous analytical framework for understanding stochastic optical solitons in highly dispersive birefringent fibers with Kerr-law refractive-index nonlinearity in the Itô sense. By reducing a coupled stochastic NLSE system through a traveling-wave transformation and carefully derived constraint conditions, the problem collapses to a single tractable ordinary differential equation. Applying the modified sub-ODE method yielded an extensive catalogue of exact analytical solutions, including bright, dark, singular, and Weierstrass elliptic structures. Among these, the present study focuses on the analysis of the bright and dark soliton solutions, while the singular and Weierstrass elliptic solutions are reported without further discussion.

These solutions illustrate how the interplay between high-order dispersion and Kerr nonlinearity governs soliton formation, while stochastic perturbations introduce phase modulation without destroying the soliton envelope. A significant outcome of this work is the stability characterization of the derived solitary waves. The obtained analytical solutions satisfy the established spectral and energy-based stability criteria, indicating that their envelope modulus remains stable under sufficiently small perturbations, whereas the multiplicative Itô noise affects only the phase evolution. This confirms the robustness of the localized wave structures and supports their physical relevance for realistic noisy birefringent optical fibers.

The results provide valuable theoretical foundations for modeling noise-driven nonlinear wave phenomena in optical fibers and related photonic platforms. The analytical solutions also serve as precise benchmarks for ultrafast pulse propagation, soliton-based communication, and the design of robust nonlinear optical systems operating under stochastic environments.

Funding and acknowledgment. Ongoing Research Funding program, (ORF-Ctr-2026-9), King Saud University, Riyadh, Saudi Arabia. This research for the last author was supported by Grambling State University for the Endowed Chair of Mathematics and is gratefully appreciated.

Author Contributions. Ahmed S. M. Metwally: Conceptualization, methodology, formal analysis, investigation. Mohamed E. M. Alngar: Validation, methodology, data curation, writing–original paper, writing–review & editing. Reham M. A. Shohib: Formal analysis, supervision, validation, investigation, writing–review & editing. Syed A. A. Shah: Methodology, software, visualization, validation. Anjan Biswas: Conceptualization, supervision, methodology, validation, funding. All authors have read and agreed to the published version of the manuscript.

Conflict of interest. The authors declare that they have no conflict of interest.

References

1. Hasegawa, A., & Kodama, Y. (1995). *Solitons in optical communications.* Oxford University Press.
2. Agrawal, G.P. (2000). Nonlinear Fiber Optics. In: Christiansen, P.L., Sørensen, M.P., Scott, A.C. (eds) Nonlinear Science at the Dawn of the 21st Century. Lecture Notes in Physics, vol 542. Springer, Berlin, Heidelberg.
3. Kivshar, Y. S., & Agrawal, G. P. (2003). *Optical solitons: from fibers to photonic crystals.* Academic press.
4. Gordon, J. P. (1987, April). Solitons in optical fibers. In *International Quantum Electronics Conference* (p. WBB2). Optica Publishing Group.
5. Akhmediev, N., Ankiewicz, A., & Soto-Crespo, J. M. (2009). Rogue waves and rational solutions of the nonlinear Schrödinger equation. *Physical Review E—Statistical, Nonlinear, and Soft Matter Physics*, *80*(2), 026601.
6. Balla, P., & Agrawal, G. P. (2018). Vector solitons and dispersive waves in birefringent optical fibers. *Journal of the Optical Society of America B*, *35*(9), 2302-2310.
7. Balla, P., & Agrawal, G. P. (2018). Nonlinear interaction of vector solitons inside birefringent optical fibers. *Physical Review A*, *98*(2), 023822.
8. Tanemura, T., & Kikuchi, K. (2006). Circular-birefringence fiber for nonlinear optical signal processing. *Journal of lightwave technology*, *24*(11), 4108-4119.
9. Latas, S. C., Ferreira, M. F. S., & Facão, M. (2017). Ultrashort high-amplitude dissipative solitons in the presence of higher-order effects. *Journal of the Optical Society of America B*, *34*(5), 1033-1040.
10. Abdelwahed, H. G., Alsarhana, A. F., El-Shewy, E. K., & Abdelrahman, M. A. (2023). Higher-order dispersive and nonlinearity modulations on the propagating optical solitary breather and super huge waves. *Fractal and Fractional*, *7*(2), 127.
11. Li, M., Xu, T., & Wang, L. (2015). Dynamical behaviors and soliton solutions of a generalized higher-order nonlinear Schrödinger equation in optical fibers. *Nonlinear Dynamics*, *80*(3), 1451-1461.
12. Zhou, Q., Zhu, Q., Liu, Y., Yu, H., Yao, P., & Biswas, A. (2015). Thirring optical solitons in birefringent fibers with spatio-temporal dispersion and Kerr law nonlinearity. *Laser Physics*, *25*(1), 015402.

13. Biswas, A., Triki, H., Zhou, Q., Moshokoa, S. P., Ullah, M. Z., & Belic, M. (2017). Cubic–quartic optical solitons in Kerr and power law media. *Optik*, *144*, 357-362.
14. Roshid, M. M., & Rahman, M. M. (2024). Bifurcation analysis, modulation instability and optical soliton solutions and their wave propagation insights to the variable coefficient nonlinear Schrödinger equation with Kerr law nonlinearity. *Nonlinear Dynamics*, *112*(18), 16355-16377.
15. Afsar, H., Peiwei, G., Alshamrani, A., Aldandani, M., Alam, M. M., & Aljohani, A. F. (2024). Dimensionless dynamics: Multipeak and envelope solitons in perturbed nonlinear Schrödinger equation with Kerr law nonlinearity. *Physics of Fluids*, *36*(6).
16. Sağlam, F. N. K., Kopçasız, B., & Ahmed, K. K. (2026). Exploration of different soliton solutions for the stochastic davey–stewartson model under the influence of noise. *Archives of Computational Methods in Engineering*, *33*(1), 1159-1179.
17. Liu, J., Li, M., He, J., Song, Y., & Wang, Z. (2023). Noisy soliton pulsation and its dynamics in a mid-infrared ultrafast fiber laser. *Chaos, solitons & fractals*, *177*, 114199.
18. Mshary, N., Bossly, R., & Ahmed, H. M. (2025). Noise effects on soliton structures of nonlinear Schrödinger equation with generalized Kudryashov's law non-linearity using modified extended mapping technique. *Scientific Reports*, *15*(1), 36949.
19. Abdelwahed, H. G., El-Shewy, E. K., Abdelrahman, M. A., & Alghanim, S. S. (2023). The noise sense effects on the characteristic nonlinearly Schrödinger equation solitary propagations. *Journal of Low Frequency Noise, Vibration and Active Control*, *42*(2), 818-825.
20. 20 Albayrak, P., Ozisik, M., Secer, A., Bayram, M., & Das, S. E. (2024). Optical solitons of stochastic perturbed Radhakrishnan–Kundu–Lakshmanan model with Kerr law of self-phase-modulation. *Modern Physics Letters B*, *38*(15), 2450122.
21. Wali, S., Munawar, M., Abdelkader, A., Jhangeer, A., & Imran, M. (2025). Nonlinear stochastic dynamics of the intermediate dispersive velocity equation with soliton stability and chaos. *Entropy*, *27*(11), 1176.
22. Shehzad, K., Wang, J., Seadawy, A. R., Arshad, M., & Ahmed, I. (2024). Dynamic description of soliton solutions of nonlinear schrödinger equation with higher order dispersion and nonlinear terms. *Physica Scripta*, *99*(12), 125284.
23. Fan, W., Liang, Y., & Han, T. (2024). Novel insights into high-order dispersion and soliton dynamics in optical fibers via the perturbed Schrödinger–Hirota equation. *Scientific Reports*, *14*(1), 31055.
24. Li, Z. L. (2010). Periodic wave solutions of a generalized KdV-mKdV equation with higher-order nonlinear terms. *Zeitschrift für Naturforschung A*, *65*(8-9), 649-657.
25. Zayed, E. M., & Alngar, M. E. (2020). Application of newly proposed sub-ODE method to locate chirped optical solitons to Triki–Biswas equation. *Optik*, *207*, 164360.
26. Zayed, E. M., Al-Nowehy, A. G., Alngar, M. E., Biswas, A., Asma, M., Ekici, M., ... & Belic, M. R. (2021). Highly dispersive optical solitons in birefringent fibers with four nonlinear forms using Kudryashov's approach. *Journal of Optics*, *50*(1), 120-131.
27. Gonzalez-Gaxiola, O., Biswas, A., Yildirim, Y., & Alshehri, H. M. (2022). Highly dispersive optical solitons in birefringent fibers having Kerr law of refractive index by Laplace–Adomian decomposition. *Optik*, *257*, 168788.
28. Yıldırım, Y., Biswas, A., Ekici, M., Zayed, E. M., Khan, S., Moraru, L., ... & Belic, M. R. (2020). Highly dispersive optical solitons in birefringent fibers with four forms of nonlinear refractive index by three prolific integration schemes. *Optik*, *220*, 165039.

Metwally, A.S.M., Alngar, M.E.M., Shohib, R.M.A., Shah, S.A.A., Biswas, A. (2026). Highly Dispersive Optical Solitons with Differential Group Delay and Multiplicative White Noise Having Kerr Law of Self-Phase Modulation. *Ukrainian Journal of Physical Optics*, *27*(3), 03196 – 03224.
doi: 0.3116/16091833/Ukr.J.Phys.Opt.2026.03196

Анотація. *У цій роботі представлено комплексне аналітичне дослідження стохастичних оптичних солітонів, що поширюються у високодисперсійних двопроменезаломлюючих волокнах, регульованих нелінійністю показника заломлення за законом Керра в сенсі Іто. Починаючи зі зв'язаної стохастичної нелінійної системи Шредінгера, що включає дисперсію високого порядку, крос-фазову модуляцію та фазові флуктуації, індуковані Вінером, для отримання детермінованого звичайного диференціального рівняння для обвідних солітонів після накладання відповідних умов обмеження використовується редукція біжучої хвилі. Використовуючи модифікований* *метод допоміжного звичайного диференціального рівняння (допоміжне ЗДУ), ми отримуємо кілька сімейств точних розв'язків замкнутої форми, включаючи яскраві, темні, сингулярні та еліптичні структури Вейєрштрасса, разом з їхніми відповідними умовами існування. Згодом аналізуються яскраві та темні солітонні розв'язки для ілюстрації впливу стохастичного збурення. Аналітичні результати показують, як ієрархія дисперсії вищого порядку взаємодіє з нелінійністю Керра для стабілізації локалізованих хвильових форм, тоді як стохастичний член Іто модифікує лише внутрішню фазу, не впливаючи на модуль солітона. Крім того, отримані сімейства солітонів задовольняють умови стійкості, демонструючи, що профілі обвідної залишаються стійкими, незважаючи на наявність мультиплікативного білого шуму. Ці результати дають нове розуміння поширення нелінійних хвиль, зумовлених шумом, у двопроменезаломлюючих оптичних волокнах та пропонують точні аналітичні орієнтири для надшвидкої фотоніки, нелінійного керування імпульсами та стохастичних оптичних систем.*

Ключові слова: *оптичні солітони, дисперсія високого порядку, двопроменезаломлюючі волокна, нелінійність Керра, числення Іто, стохастичне нелінійне рівняння Шредінгера, модифікований метод допоміжного звичайного диференціального рівняння*